Radar remote sensing for detecting and mapping of shellfish distribution on intertidal flats in the Dutch Wadden Sea

LYDIA BIRI NASIMIYU
February, 2018

SUPERVISORS:
Drs. E. H. Kloosterman
Dr Yousif A. Hussin

Radar remote sensing for detecting and mapping of shellfish distribution on intertidal flats in the Dutch Wadden Sea

LYDIA BIRI NASIMIYU
Enschede, The Netherlands, February, 2018

SUPERVISORS:
Drs. E. H. Kloosterman
 Dr Yousif A. Hussin

ADVISORS
Drs. Eduard Westinga
PROF.DR.IR. R.F. (Ramon) Hanssen - TU DELFT

THESIS ASSESSMENT BOARD:
[Dr. A.G. Toxopeus (Chair)
[Zulkiflee Abd Latif (External Examiner, University Technology MARA Malaysia)

ABSTRACT

The Wadden Sea is an most important inter-tidal flats in the world because of its rich biodiversity. Here, shellfish beds act as indicators of a healthy ecosystem. Therefore, there is a need to monitor shellfish beds' type and species composition. Synthetic Aperture Radar (SAR) remote sensing has the advantage of penetrating through cloud cover as compared to optical sensors, which makes it applicable on overcast as well as in the night. Shellfish beds, composed of two species - oysters and mussels, have the structural characteristic of protruding from the substrate, that enables them to be detected by SAR imagery. This study sought to detect, map and identify shellfish beds' species in the Dutch Wadden Sea by assessing the characteristics of available polarisation in SAR scenes. The study also determined the spatial variation of surface roughness (rugosity and height) of the shellfish beds. RADARSAT 2 and the recent upgraded SENTINEL 1 obtained for low tide scenes were used to detect shellfish beds with different polarisations. HH, VV and HV polarizations were available from three images. Shellfish density, shellfish height and rugosity index (field surface roughness) were obtained for each field plot of size 10m by 10m. Variograms were used to measure the degree of spatial autocorrelation using a 5 by 5-pixel window, which was a representation of 25m by 25m of a shellfish bed. VV and HH had strong relationships (p=0.05) with shellfish density at $R^2=0.72$ and HV with $R^2=0.59$ respectively. However, it was not possible to discriminate between species. The two species are rarely pure species in the beds, and the ANOVA results show that both species show the same range of SAR backscatter values variation. There was a weak spatial autocorrelation within a shellfish bed, hence demonstrating a weak significant (p=0.05) relationship with field parameters (rugosity index of $R^2=0.33$, shellfish density of $R^2=0.2$ and shellfish height of $R^2=0.18$). However, a larger subset of 2km by 2km showed a strong degree of spatial autocorrelation from one shellfish bed to another. When mapping, kriging interpolation results showed a high degree of spatial autocorrelation of 117m range with an RMSE ≈ 0.9m. Additionally, a new, reclassified HV polarized image from collocated VV and HH displayed well the brighter backscatter values relating to 2016 shellfish bed vector data. Even though there was no accuracy assessment done, the reclassified image shows that 2016 polygons were larger than identified shellfish areas suggesting that there were no clear boundaries. Hence there should be an increase in sampling frequency to increase the training samples for easier mapping of the distribution of shellfish beds.

Keywords: Tidal flats, mussel, oyster, SAR, polarisation, backscatter, rugosity index, variogram and spatial autocorrelation

DEDICATION

This work is dedicated to my dear grandmother Berita Wekesa, who sacrificed a lot to ensure I reach where I am today.

ACKNOWLEDGEMENT

LIST OF ACRONYMS

dB	Backscatter
GRD	Ground Range Detected
HH	Horizontal send, Horizontal receive
HV	Horizontal send , Vertical receive
IMARES	Wageningen Marine Research
LiDAR	Light Detection And Ranging
RADAR	Radar Detection and Ranging
RSC2	Radarsat C band Images
SAR	Synthetic Aperture Radar
SC1	Sentinel C band Image
SLC	Single Look Complex
SNAP	Sentinels Application Platform 2
SNR	Signal to Noise Ratio
TMAG	Trilateral Monitoring and Assessment Group
VV	Vertical send, Vertical receive
WaLTER	Wadden Sea Long-Term Ecosystem Research
WSP	Trilateral Wadden Sea Plan

TABLE OF CONTENTS

LIST OF FIGURES

LIST OF TABLES

LIST OF APPENDICES

1.   INTRODUCTION

1.1 Background and Justification

The Wadden Sea is the largest continuous tidal flat ecosystem in the world (World Numismatic News, 2017). It was designated a UNESCO Heritage Site in 2009, a Natura 2000 site under both the EU Birds and Habitats Directives (Marencic, 2009). Before that, it was listed under the Ramsar Convention (Horstmann & Koch, 2008). It spans across three countries, Netherlands, Germany, and Denmark – in northern Europe covering a total area of about 10,000 km² (Brockmann & Stelzer, 2008).

The Wadden Sea's unique geomorphological features are habitats for vibrant, rich biodiversity. For example, every year 10-12 million migratory birds make a stopover before they continue with their journey to other stops in Africa and the Mediterranean. It hosts a wide variety of plant and animal life, occupying specific niches along different gradients. Notably, it is a habitat to shellfish that are important in determining the function and community composition of tidal flats. Shellfish increase benthic primary production by speeding up nutrient cycling and also promote the reduction of hydrodynamic forces influencing the sediment properties (Ens, 2003; Folmer *et al.,* 2014).

During the last decades, anthropogenic activities such as overfishing, pollutants from farm nutrients, other chemicals, and hydraulic engineering have negatively impacted the Dutch tidal flat ecological status (NIOZ, 2017). Overfishing is believed to be the main human activity that resulted in declines of mussel populations since the year 1990 (Ens, 2003). Siltation from the western side of the Wadden Sea has also reduced the suitable conditions for Blue mussel (*Mytilus edulis*) production. The impact of ship transports and other offshore human activities have also contributed to the deterioration of this intertidal ecosystem. Furthermore, winter temperatures have also been observed to increase the mortality rate of shellfish. These events have contributed to declining of waterfowl in the tidal flats (Ens, 2006; Daskalov *et al.,* 2007; Thorup & Koffijberg, 2016).

In the year 1991, the Trilateral Monitoring and Assessment Group (TMAG) developed the Trilateral Wadden Sea Plan (WSP), aimed at monitoring the Wadden Sea ecosystem. This entailed the incorporation of management policies and programs of the three countries (Netherlands, Germany, and Denmark) as mandated by Natura 2000 . This intervention was in compliance to EU Bird and Habitats Directives policy in protecting the Wadden Sea (Sundseth, 2014). Effective monitoring and assessment of tidal flats need safe accessibility. At the Wadden Sea, access has been a challenge because of the limited window in time of low tide to access the region. Furthermore, labor-intensive methods such as the data collection in estimation of shellfish beds are needed to determine the ecological status of these flats. These methods are also very time-consuming (Common Wadden Sea Secretariat, 2008).

Recent monitoring along the tidal flats include the Wadden Sea Long-Term Ecosystem Research (WaLTER) project that has developed a satellite imagery monitoring plan for the region to address the limited low tide window of two hours (Davaasuuren *et al.,* 2014). The use of remotely sensed satellite imagery is advantageous in that the images can be obtained more frequently. Optical remote sensing has been used in estimating primary production (Morris, 2005) and in distinguishing live and dead oysters reefs from a Floridian Lagoon (Grizzle *et al.*, 2002). Hyperspectral remote sensing, on the other hand, has been used in estimating the types of sediments in the tidal flats (van der Wal & Herman, 2007). The use of these technologies would be limiting at Wadden Sea because they only detect the upper layers the shellfish

beds and cannot be practically operational in areas with heavy cloud cover such as the Wadden Sea (Brockmann & Stelzer, 2008).

The Radio Detection and Ranging (RADAR) remote have been employed to overcome the cloud cover challenge hence providing an alternative for detecting shellfish in the Wadden Sea. The radar waves can penetrate through clouds and thus an all-weather type of sensor that allows observation of earth cover at any time of the day (day and night) with high-resolution images (Jung *et al.,* 2015). A transmitted pulse from the wave interacts with an object or surface to form a backscatter signal. This signal depends on permittivity and surface roughness. In the ocean, the differences in backscatter enable the detection of ocean waves, sea surface and ocean currents (Klemas, 2014; Adolph *et al.,* 2017).

Synthetic Aperture Radar (SAR) is a type of RADAR that creates two / three-dimensional images of the detected object. In the Dutch Wadden Sea, the use of SAR remote sensing allows the differentiation of the shellfish beds from the surrounding. The beds are mostly categorized using characteristic physical features such as the surface roughness(Gade *et al.,* 2014; Nieuwhof *et al.,* 2015). The beds have been captured in SAR images across different wavelengths due to their differences in surface roughness of the beds compared to the roughness of surrounding sediments along the German Wadden sea (Gade *et al.,* 2010). Furthermore, Choe *et al.* (2012) demonstrated that backscattering characteristics could distinguish between oyster reefs and mudflats in the Korean Peninsula.

Surface roughness has been measured manually in coral reefs and soil surfaces using the rugosity index measurement. This is index measures the variations of the height of a surface at a selected sample plot (Saleh, 1993).In a spatial scale, variogram may be used to determine a degree of spatial variation. Variogram characterizes the variation of objects and surfaces between two locations in a spatial scale(Morris, 2005).

Estimation of the distribution of shellfish beds with a specific focus on their variation using SAR imagery was the aim of this study. Manual field measurements of the estimated shellfish density, shellfish height, and rugosity were also made as independent variables to correlate with analyzed SAR images so as to determine if the SAR signal can discriminate the shellfish beds from the surrounding.

1.2 Problem statement

The condition of shellfish beds is a good indicator of the ecological status of the Dutch Wadden Sea. Shellfish bed monitoring is needed to determine the Dutch Wadden sea conservation trend with the human use impact. The tidal flats have a two-hour window to be accessed per day. Subsequently, the area is prone to cloud cover which limits the use optical imagery that is commonly used in monitoring. For these reasons, SAR remote sensing is advantageous in penetrating through cloud cover. Spatial variation analysis may be used in differentiating shellfish beds and surrounding. It is therefore important in distinguishing tidal flats features by first visualizing the distribution of shellfish beds in different polarisations. Second, correlating with shellfish density and lastly, determining the degree of spatial autocorrelation within beds before the complex using models.

1.3 Research objectives

1.3.1 General objective:

This research aimed to detect, identify two shellfish species and map their spatial distribution and density in the Dutch Wadden Sea using SAR imagery.

1.3.2   Specific objectives:

1. Assess the characteristics of polarisation of SAR backscatter from shellfish beds with different densities and species composition on the surrounding tidal flats.

2. Map the spatial distribution and density of shellfish beds at species level with SAR imagery.

1.3.3   Research questions

1) Is the backscatter signal of SAR image associated with;

    a. Presence of shellfish beds?

    b. The density of shellfish beds?

    c. The species composition of shellfish beds?

2) Is the backscatter signal variation associated with shellfish density and surface roughness (rugosity and height)?

3) How accurate can SAR data;

    a) Map shellfish beds distribution and density?
    b) Map shellfish beds distribution and species composition?

1.3.4   Research Hypotheses

1) H_0: There is no significant difference in the radar backscatter signal of different polarisations with shellfish densities.

2) H_0: There is no significant difference in the radar backscatter signal with species composition.

3) H_0: There is no significant relation between backscatter signal variation with shellfish density and surface roughness (rugosity and height).

2. THEORETICAL BACKGROUND

In this chapter, the principles and opinions of various researchers on radar sensitivity are presented. It further explains the application of radar in different areas and its integration with other applications in the tidal flats.

2.1 Radar backscatter sensitivity

Radar backscattering is determined by the reflective strength of the targeted object and the alignment of an object in relation to the radar antennae From each pixel; there is a backscatter value obtained in relation to the type of the object (Adolph *et al.,* 2017). In coastal mapping, the backscatter signal is determined by the dielectric constant, surface roughness and other parameters such as salinity, porosity, moisture; and slope. Factors affecting radar discussed in this chapter include wavelength, polarisation and surface variations. Equation 2-1 shows the relation between backscatter and surface roughness.

Equation 2-1

$$h < \frac{\lambda}{8.\cos\theta}$$

Where by
h = mean height of surface variations
λ =Wavelength
θ =Incidence angle

2.1.1 Wavelength

There are different types of SAR bands ranging from Ka to L band as shown in Figure 2-1 with the wavelength ranging from 1mm to1.3m wavelength . X band ranges between 2.8–5.2 cm, C- (4.8–7.7 cm), L- (15–30 cm) and P band range between (30–100 cm). Studies have shown that X band has a stronger radar backscatter as compared to other bands . This is because X band is advantaged to have a shorter wavelength as compared to C- and L-bands. Hence, an increase in wavelength weakens the effect of radar backscatter hence the shorter the wavelength the higher the backscattering (Lee *et al.,* 2012; Gade *et al.,* 2014; Nieuwhof *et al.,* 2015; Gade & Melchionna, 2016; Gade *et al.,* (2017); Wang *et al.,* 2017).
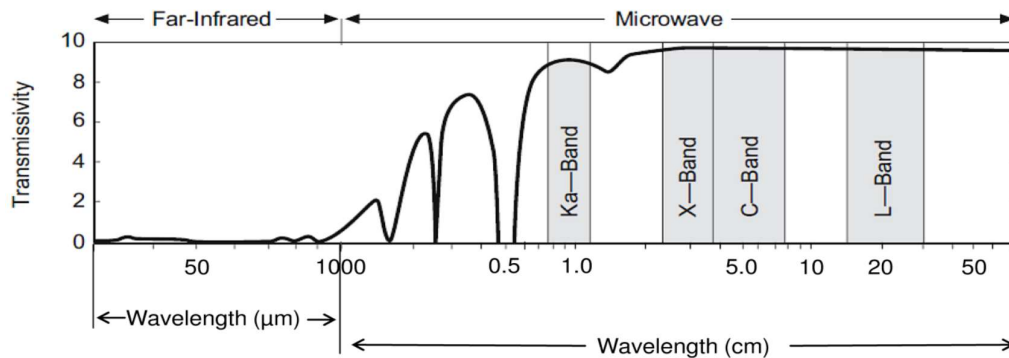
Figure 2-1: Radar electromagnetic spectrum (changed after Lusch 1999)

2.1.2   Types of scattering

SAR signal returns from the object in four ways; namely, i) specular scattering whereby there is no return to the sensor, occurring in smoother surfaces such as bare soil and water. ii) rough scattering is as a result of single bounce to the sensor such as soil. iii)volume scattering is as a result of multiple scattering from objects such as forest canopy. iv) double-bounce scattering is a result of two right-angled smooth surfaces deflecting incoming SAR signal of the surfaces, thus resulting to most energy returning to the sensor such as vertically emerged vegetation of a clear, smooth water surface(Chandola, 2014).

2.1.3   Polarisation

Polarisation is the transmission and reception of the magnetic wave. It is determined by amplitude and the type of the wavelength. Polarisation identifies the orientation angles with ellipticity and shape of the object. As a result, transmission and reception are either in horizontal (HH), transmission and reception in vertical (VV) or in H transmission and V reception (HV) or V transmission and H reception (VH). Also depending on the transmitter, it can relay single, cross or dual polarisations. These types of polarisations produce different backscatter results of the same object. For instance, a linear vertical polarisation is usually indicated at the center of the plot while the horizontal polarisation is at the center of X-axis (see Figure 2-2) (Durden *et al.,* 1989).
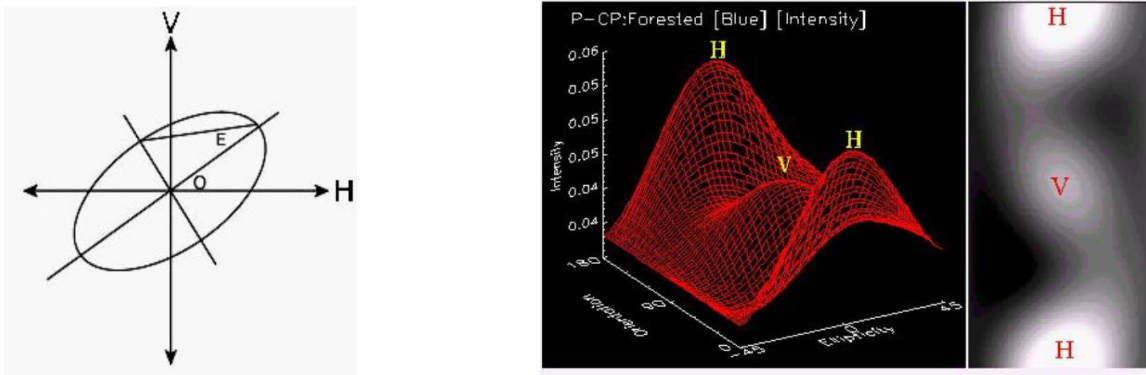
Figure 2-2: Left shows the Polarisation ellipse (E- ellipticity angle , orientation angle –O) , V and H show the direction of the radar transmitted signal, right shows a forested region of P-band AIRSAR data of H and V linear polarizations.

2.1.4   Surface variations

On a smooth surface, the radar energy may bounce away, which means little may return to the antenna. A similar scenario occurs with a wet surface. Hence the outcomes will show high reflection (specular reflection) and less backscatter resulting in dark areas in SAR images (ESA, 2017). In practical, wetland surroundings (sand, vegetation, and rock) can be differentiated from the water. This is because sand, vegetation, and rocks will cause multiple scattering thus resulting to high backscatter : the reflections will display as brighter areas in the SAR images) (Cooley & Barber 2003). A similar result is obtained in tidal creeks along the coast whereby the higher backscatter is seen along their edges (Deroin, 2012).

Shellfish beds have a unique shellfish height of variations. This is a unique characteristic that causes multiple scattering resulting in high backscattering effect (Gade *et al.,* 2008; Gade *et al.,* 2010). To

differentiate shellfish species' beds, Melchionna and Gade (2014) recommended the need to use parallel banks of shellfish beds. The different species of shellfish beds when parallel to each other allows observation of the different range in backscatter values.

Other than tidal flats, SAR remote sensing has been applied in other areas such as from crop modeling and forest mapping as summarized in Table 2-1.

Table 2-1: Modelling and mapping, an overview of selected studies of radar application in various sites

Radar Dataset	Study Area	Techniques	Reference
TerraSAR-X, RADARSAT-2 (C-band)	Dutch Waddensea	Integral Equation Model for Shellfish Backscatter Modelling and Mapping	(Nieuwhof *et al.,* 2015)
TerraSAR-X	German Waddensea	Textural Analysis for Spatiotemporal Analysis of Bedforms Dynamics	(Adolph *et al.,* 2017)
TerraSAR-X, RADARSAT-2 (C-band)	German Waddensea	Temporal Statistics in Relation to Polarization Coefficient and Band Coefficient	(Melchionna & Gade, 2014)
TerraSAR/TanDEM-X	German Waddensea	Archaeological Surveys	(Gade *et al.,* 2017)
ALOS PALSAR L band, ENVISAT ASAR C band	Ghana forest	Regression Modelling for Estimation of Above Ground Biomass	(Nga, 2010)
Sentinel-1 C band	Romania plains	Soil and Vegetation Indices Correlation Analysis	(Poenaru *et al.,* 2015)

2.2. Integration of remote sensing methods for shellfish detection

The Integral Equation Model (IEM) is a model used to measure surface roughness for a specific area while incorporating surface autocorrelation information. IEM is mostly used in measuring soil moisture, soil type and also shellfish beds (See Figure 2-3.). Whereby the autocorrelation function (length) determines the relation between surface heights , and the root mean square height (RMS(z)) determines the standard deviation of different heights of the surfaces (Deroin, 2012).
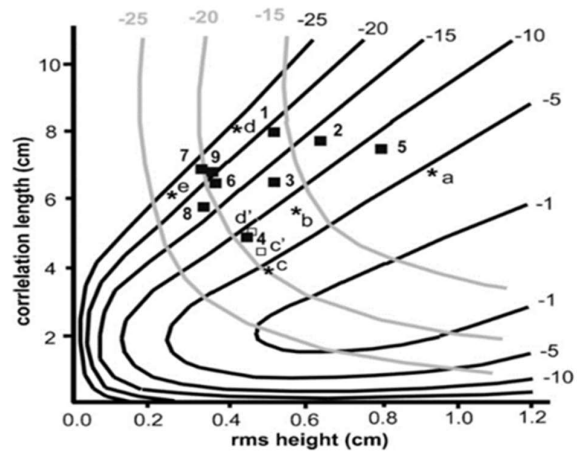
Figure 2-3: An example of RMSz and correlation length obtained from ALOS PALSAR(L-Band –black lines), ERS-2 SAR (C band- grey lines). a, b and c show different soil types (Deroin, 2012).

SAR images are usually affected by speckles noise (salt and pepper) (Goodman, 1976) that reduces the accuracy of the processes carried out (Goodman, 1976; Lee, 1999). Therefore, there is need to filter the images and also use other remote sensors to get better results. Aerial photography can be used hand in hand with SAR images to compare objects of the same coordinates (Koch *et al.,* 2012). Furthermore, visual interpretation of black & white and false-color aerial photography has been used in habitat mapping and discrimination of shellfish beds (Mumby *et al.,* 1997; Roberts *et al.,* 2003; Harris & Baker, 2012). In this research, the use of aerial photography was key in the identification of shellfish beds for fieldwork purposes along the Dutch tidal flats.

3. STUDY AREA

3.1 Location

The study was conducted in Dutch Wadden Sea along the shores of Ameland and Terschelling Islands, and on the mainland parts of Groningen and Friesland provinces (see Figure 3-1). It borders the Northern Sea in the North West of the Netherlands. The whole Wadden Sea covers an area of 10,000 km², with salt marshes and intertidal flats covering 5,300 square kilometers (Dankers *et al.,* 2012) It has a two-hour window period for low tide twice a day. The gentle slopes and steep bank forming creeks increase the variation of sediment types. Thus, creating shores of mainland and Ameland Island to have a high content of mud whereas Terschelling island with pure sand.

The Wadden Sea is surrounded by inhabited islands that have salt marshes, Pleistocene cliffs, dune islands and sea walls with three major estuaries - Rivers Elber, Weser and Ems (van Roomen *et al.,* 2012). The low intertidal zones act as habitats for *M. edulis* and *C. gigas*. Suspension feeders filter the tidal water creating a suitable habitat for other species such as sessile invertebrates and more than 140 fish species (Wolff *et al.,* 2010). It also harbors more than 10 million migratory birds that use these sites for breeding, roosting, feeding and refueling for the next journey. The main predator waterfowls are black-headed gull (*Chroicocephalus ridibundus*), Eurasian oystercatchers (*Haematopus ostralegus*), European herring gull (*Larus argentatus*) and dunlin (*Calidris Alpina*) onto which they feed mainly on polychaetes, crustaceans, and shellfish (Nehls & Thiel, 1993; Colwell, 2010).
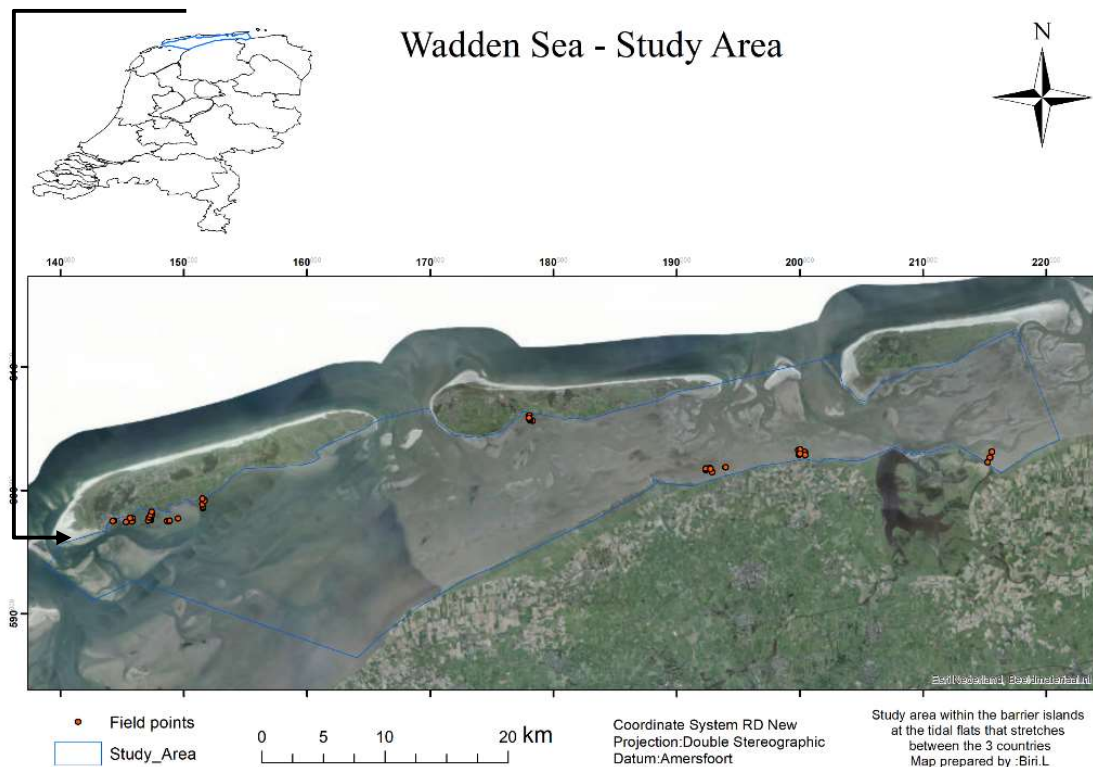
Figure 3-1: Aerial photograph showing the location of Dutch tidal flats in and distribution of 50 field sample areas.

3.2 Shellfish Species

M. edulis population is an endemic species in the Wadden Sea whereas *C. gigas*; is an exotic species originally from Japan(see Figure 3-3) *M. edulis* beds have a total area of 2052 ha while *C. gigas* reefs have a total of 1455 ha. Their population is determined by the tidal flat abiotic conditions. They are also indicators of high biodiversity acting as habitats for other benthic invertebrates in the marine food chain (Nehls *et al.,* 1997; Nehls & Büttger, 2007). However, birds prefer to feed on *M. edulis* rather than on *C. gigas* because of their soft tissue that eases the swallowing process.

Aerial photographs from 1990 in combination with 2007 field observed transects of the Wadden Sea show of an increase in distribution *C. gigas* reefs and reduction of *M. edulis* beds (Fey *et al.,* 2007). This trend is because of *M. edulis* beds that tend to be constant over a period and also regrow from the old beds (Nehls *et al.,* 1997). Intensified fishing in combination with slow recovery has led to declining of *M. edulis* in the Wadden Sea (Dankers *et al.,* 2001). Sediment disturbance has affected the primary production of macro algae and seagrass onto which are depended by *M. edulis* for production and their recovering rate (Eriksson *et al.,* 2010).

C. gigas reefs, on the other hand, are known to overgrow on top of other shellfish species such as the *M. edulis*. Moreover, environmental changes favor larvae of *C. gigas,* especially under warm winter conditions thus increasing the spread of oyster reefs on the tidal flats (Nehls *et al.*, 2006).In all their life cycle stages, C. *gigas* have traits described in Figure 3-2). that initiate and make them fit and enables them to flourish in a new environment (Troost, 2009). However, oyster reefs are also affected by unstable weather patterns such as storms and waves that promote the increase of parasites and diseases. These also reduce the health of oyster reefs (Ens, 2006; Fey et *al.*, 2007 ; Nehls & Büttger, 2007; Van Den *et al.*, 2016).

Stage	Trait
Colonization	rapid growth
	rapid sexual maturation
	high fecundity
	ability to colonize wide range habitat types
	broad diet
	tolerance to wide range environmental conditions
	gregarious behaviour
	genetic variability & phenotypic plasticity
	ability to recolonize after population crash
Establishment	competitiveness
	lack of predators, parasites and diseases
	association with humans
	repeated introductions
	ecosystem engineering
	genetic variability & phenotypic plasticity
Natural range expansion	dispersability
	traits of successful colonists (see above)

Figure 3-2: Characteristics of successful invader- Oyster : source (Troost, 2009)

Blue Mussel
(*Mytilus edulis)*

Pacific Oyster
(Japanese oyster:
Crassostrea gigas)

Figure 3-3: common Blue mussel and Japanese oyster ; these are the most common shellfish species found in the Wadden sea.

4. MATERIALS AND METHODS

4.1 Methodological Steps

To answer the research questions, Field data was collected to meet the four main methodological steps.
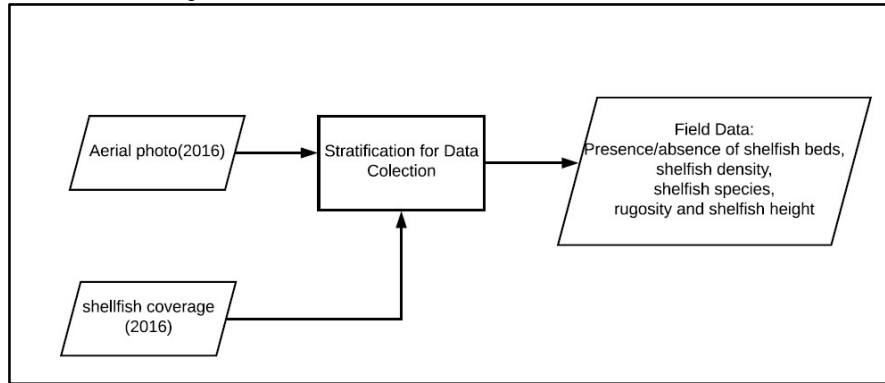
Figure 4-1: Stratification of accessible shellfish beds and data collection

1. Visual assessment of the relation between the presence of shellfish beds and the backscatter intensity of the SAR images(see Figure 4-2).
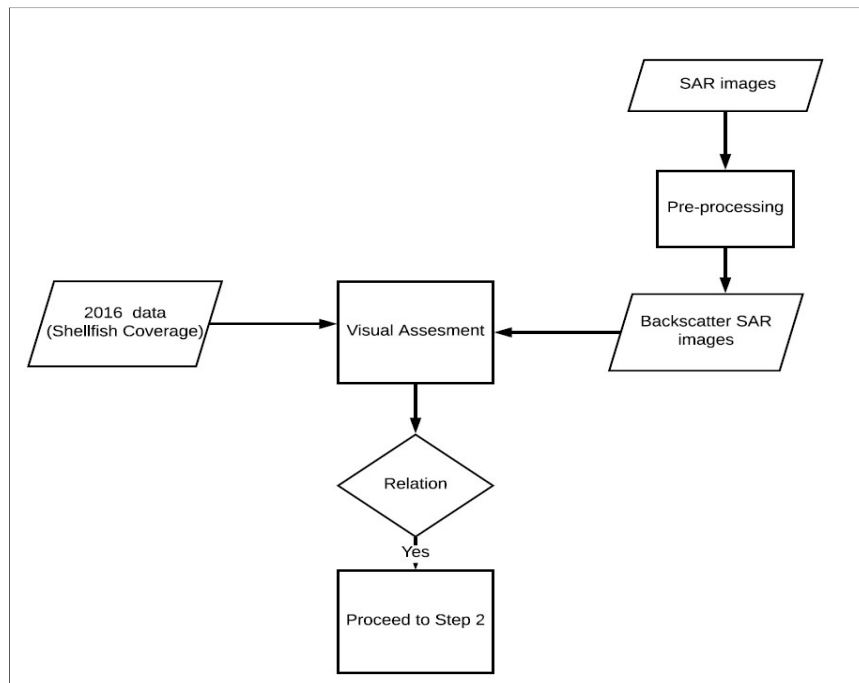
Figure 4-2: Flowchart: Detecting presence and absence of shellfish

2. Assess the relation between the density of the shellfish beds and the backscatter signal in different polarisations (see Figure 4-3).
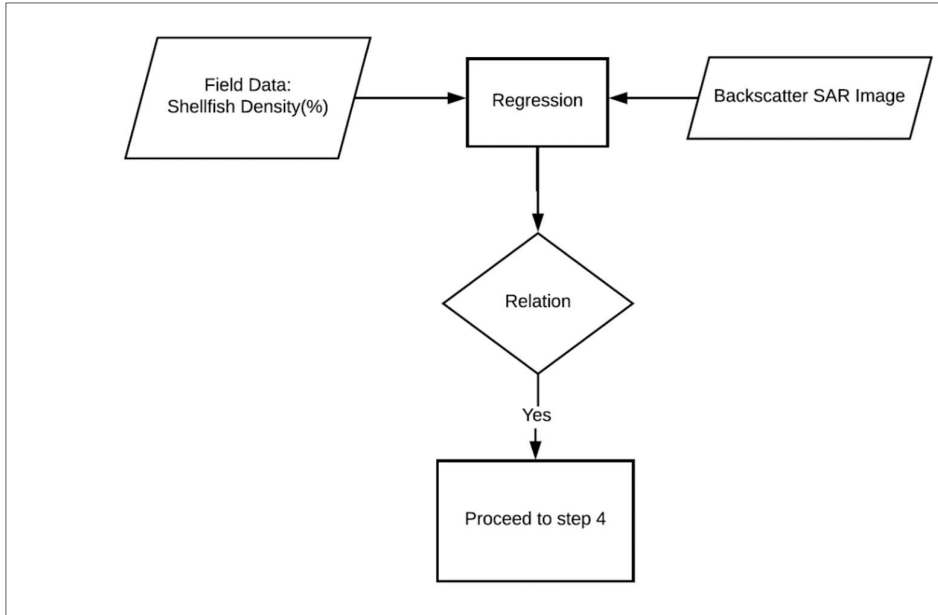
Figure 4-3: Flowchart: Relation between shellfish and backscatter signal

3. Asses the relation between shellfish species with the backscatter signal(see Figure 4-4)
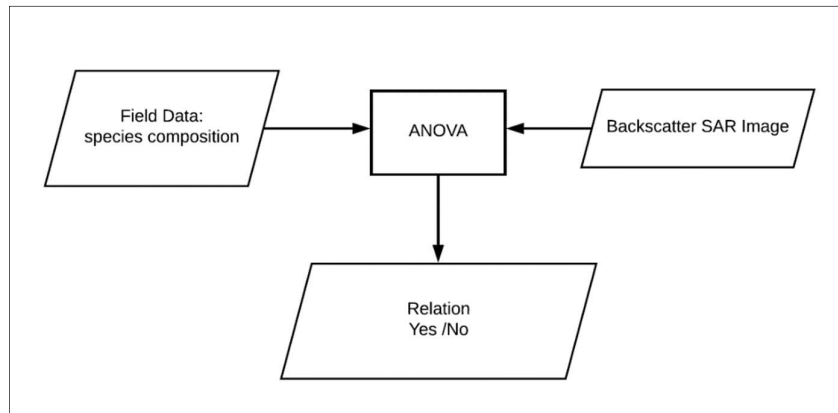
Figure 4-4: Flowchart : Relation between shellfish species with the backscatter signal

4. Assess the relation between spatial variability of the backscatter signal and shellfish characteristics (see Figure 4-5).
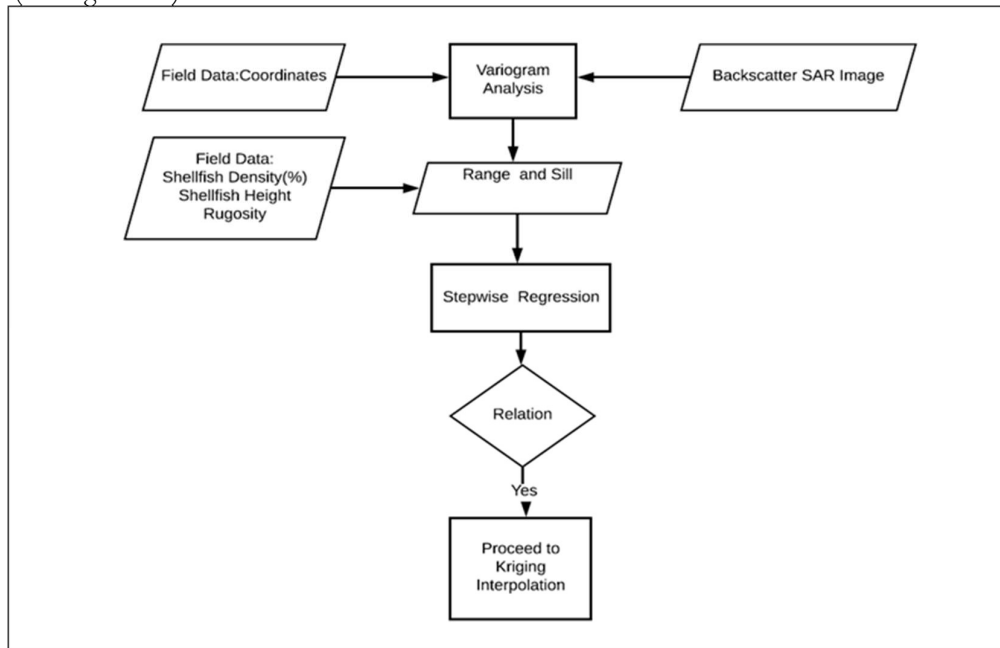
Figure 4-5 Flowchart: Semi-variogram Analysis

5. Estimate shellfish cover (see Figure 4-6)
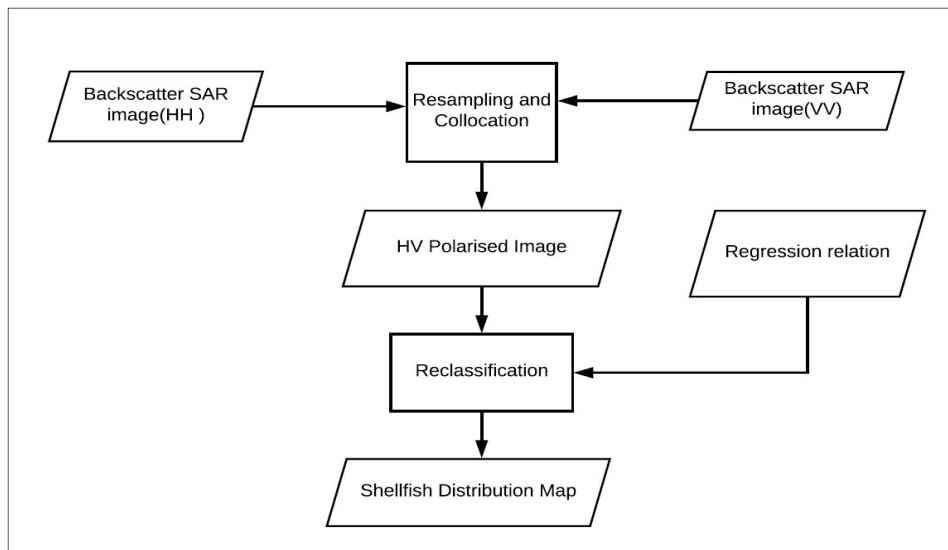
Figure 4-6: Flowchart: Mapping Shellfish beds

4.2 Overview of the data.

An overview of the data used for this study as shown in Table 4-1.

Table 4-1: Specifications of different SAR products and other data acquired. SLC is Single Look Complex, and GRD is Ground Range Detected. The tide information was acquired from Rijkswaterstaat - water management agency in the Netherlands.

Type	Mode	Image Date	Time	Pixel Resolution (m)	Polarization	PASS	Water Height (m AOD*)	Tidal Stage	Source
RS2/C	Extra fine: SLC	14th May 2017	18:21	4	VV	Ascending	-1.25	Low	Canadian Space Agency
RS2/C	Extra fine: SLC	25th July 2017	18:20	4	VV	Ascending	-1.61	Low	
S1A/C	Strip-map : GRD	9th June 2016	18:20	10	HH/HV	Descending	-0.69	Outgoing	ESA Scientific Hub
Aerial photograph	2016		Dutch Luchtfoto						ESRI Database
Shellfish Coverage	2016	Vector							IMARES
Tide tables	Rijkswaterstaat (https://www.rijkswaterstaat.nl/water/waterdata-en-waterberichtgeving/waterdata/getij/index.aspx)(Rijkswaterstaat, n.d.)								

4.2.1 SAR images

The images were selected two hours before and after low tide (see Table 4-1). RADARSAT-2 SAR images were acquired from Canada's RADARSAT satellite from the Technical University of Delft database. The RADARSAT satellite has a full polarization mode and a single polarization of 3m ground range mode. It has two channels of H- horizontal and V- vertical. Mode shows the resolution of pixel size. In this research extra fine mode, a high-resolution image type was used (MDA, 2016). SENTINEL 1 SAR image was downloaded from ESA Scientific Hub, an open source site. SENTINEL 1 satellite has a single and dual polarisation (ESA Earth Online, 2017). Table 4-2 shows a summary of description characteristics of the discussed radar satellites. In this research, Radarsat-2 C band will be coded as 'RSC2' and Sentinel-1 C band and 'SC1' for simplicity.

Table 4-2: Characteristics of Strip map SENTINEL 1 (ESA Earth Online, 2017) and extra fine RADARSAT 2 C Band (MDA, 2016).

Characteristic	Sentinel-1-C Band	RADARSAT-2 –C Band
Wavelength	5.405 GHz	5.405 GHz
Incidence angle range	18.3° to 46.8°	22° to 49°
Azimuth and range looks	Single	1 x 1
Types of Polarisation	Dual HH+HV, VV+VH Single HH, VV	Single Co or Cross (HH or VV or HV or VH)
Maximum Noise Equivalent to Sigma Zero (NESZ)	-22 dB	-21$\pm$2.5 dB
Radiometric accuracy	1 dB (3σ)	1 dB (3σ)
Phase error	5°	<3o

4.2.2 Aerial Photographs

The latest aerial photographs available were up to 2016.

4.2.3 Vector files

IMARES has published a GIS coverage of the distribution of shellfish and their properties based on the estimated percentage of shellfish beds per site as shown in Table 4-3). This data was received from IMARES as a shapefile. The data was collected by Wageningen Marine Research as a part of the statutory fisheries research tasks commissioned by the ministry of economic affairs.

Table 4-3: Legend of 2016 shellfish coverage (%)

No	Type of Class	Estimated Percentage
1	Mussel bed	mussels cover >5%and oysters cover <5%
2	Oyster reef	oyster cover >5% and mussel cover <5%
3	Mixed shellfish bed	oyster cover >5% and mussel cover >5%
4	Scattered shellfish	Shellfish cover <5%
5	Sediments (sand, mud seagrass, and algae, tubeworms)	sediment =100 >=95% Other Benthic

4.2.4 Tide tables

The tide tables played an important role in the identification of suitable time for image acquisition and fieldwork.

4.3 Fieldwork

- *Sampling design*

To find a relation between variation in the backscatter signal on the SAR images and the situation on the field, a stratified purposive sampling design was adopted. This design was intended to cover sediment and shellfish beds of a sampling site.

- *Selection of the sample sites*

Prior to the field work, the 2016 vector files of shellfish coverage were superimposed on the aerial photographs (stratification) to pre-select suitable sites for sampling. Within the pre-selected sampling sites, a homogeneous area of 25m x 25m was selected, and within that area, a sample plot of 10mx10m was chosen as shown in Figure 4-7.
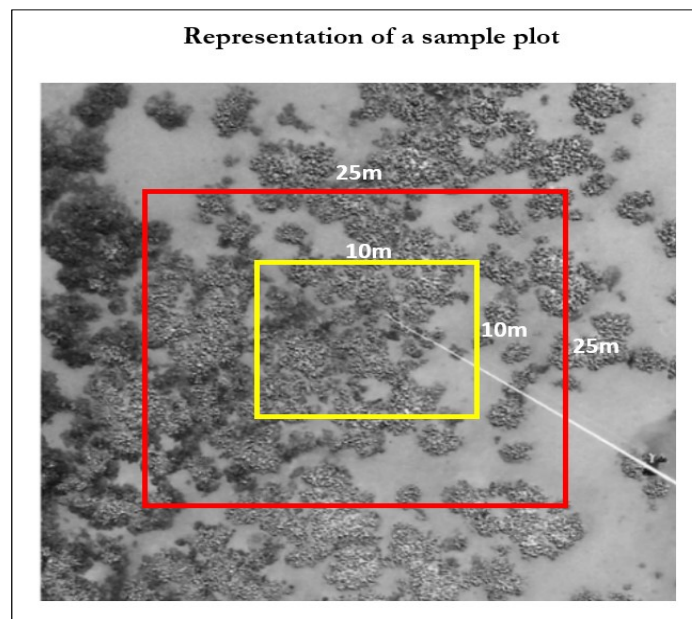
Figure 4-7: A represents a sample representation of a sample plot(Aerial photograph of part of the oyster bed at Neeltje Jans, the Oosterschelde estuary (courtesy Johan van de Koppel). The picture shows patches of oysters, and bare patches in between (Adapted from Troost, 2009)

N.B. Selection of the actual sampling sites in the field was determined by accessibility in terms of walking distance from the coast and the tide. Not all pre-selected sites could be reached. Therefore, almost all samples are close to the shores.

- *Collected field data*

Fieldwork was conducted between 16th September 2017 to 1st October 2017. In every sample plot, the following data were recorded: (see Appendix 3)

1. X, Y coordinates of the center point were collected using Garmin GPS map 78 with an average error of 5m (Dutch RD New, EPSG 28992).

2. Cover percentage of shellfish per species (mussel and oyster), algae, sediment and water of the area was collected through visual estimation.

Afterwards, 2016 vector data legend in Table 4-3 was used to quantify types of classes shown in Appendix 4. Figure 4-8 to Figure 4-11 illustrates the types of shellfish beds present in the tidal flats of the Wadden Sea.The spatial distribution of classes differs from one bed to another. Mixed shellfish beds are dominated by oysters.

Figure 4-8 : Photo of an Oyster reef with a density of 80% near Ameland Island

Figure 4-9: Photo of a Mussel bed with a density of 70% near Terschelling Island

Figure 4-10 : Photo of scattered shellfish bed with a density of < 10% near Terschelling Island

Figure 4-11: Photo of 85% Mixed shellfish bed with a density of 85% near in Ameland Island:

3. Rugosity index measurement.
Prior to the field work two different types of chains were tested to see which type would best follow the roughness of the surface. The small bead better followed the roughness chain as compared to the larger chain.

Table 4-4: Test results per chain type used for rugosity measurement

Chain type		10(m)	20(m)
Larger chain (2cm pitch 0.8cm pitch)		9.9	19.82
Small bead chain		9.82	19.75
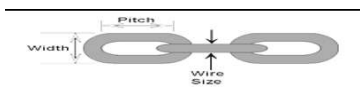
Assumptions :

1. Areas that have high shellfish density would lead to high rugosity.
2. The transmitted SAR signal information determines the smoothness or roughness of a surface. Hence high surface roughness (rugosity) will increase the roughness backscatter.

Rugosity was measured by draping a 10m long chain over a sample plot in N-S, and W-E direction and the distance between beginning and end of the chain was measured with a measuring tape. The more rugged the surface, the shorter the distance(Saleh,1993)(See Figure 4-12).The difference between the length of the chain (10m) and the distance between beginning and end point was used to calculate the rugosity index (see equation 3.1). The rugosity measurement results were later related to the spatial variation of surface roughness in SAR images.
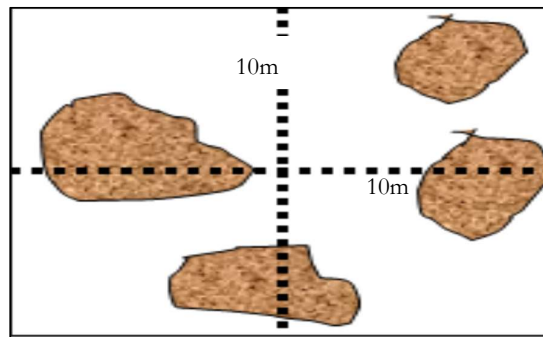
Figure 4-12: Rugosity measurement of 10m length in N-S and E-W direction across a plot.

Equation 4-1

$$C = 1 - \left(\frac{d}{I}\right)$$

C   *rugosity index,*
d   *the horizontal distance of the chain*
I   *the measuring tape length.*

4. Shell Height

Lastly, from 10 random selected shells, the height (number of cm above the substrate) was measured. The assumption taken in this measurement is that the increase shellfish height will result in high rugosity index.
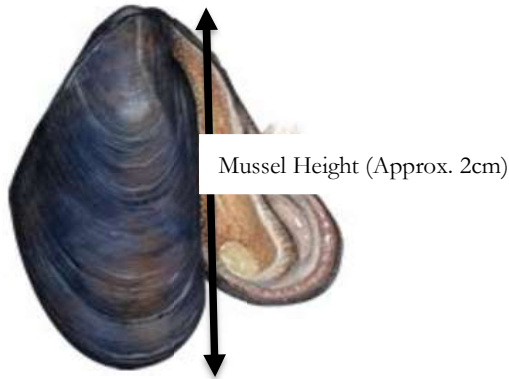
Figure 4-13:Mussel Height measurement
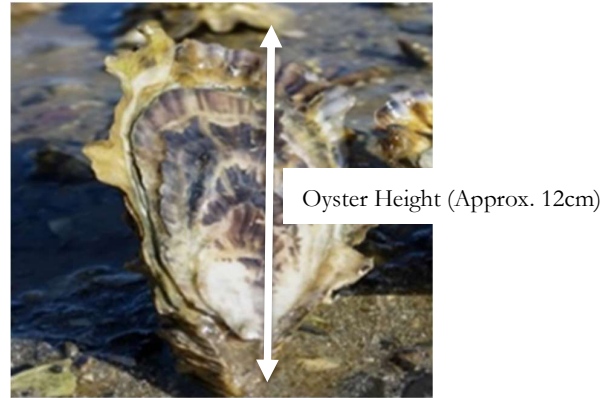
Figure 4-14:Oyster Height measurement

4.4 Pre-processing of the SAR images

The images were pre-processed using ESA's SNAP toolbox. Radarsat-2 imageries were first stacked followed by co-registering of images to one another, using the lowest tide image as a master to form a multi-temporal layer stack. Calibration of the radar backscatter was done to convert pixel value to actual backscatter values in sigma naught (σ°). One time multilooking process was performed for averaging range and azimuth resolution cells from a slant to the ground range. This was followed by Doppler terrain correction done to minimize geometry effects from the satellite. Speckle reduction was performed using 'Lee's refined adaptive,' a local filter of 7×7 moving windows. Speckle reduction in SAR images also affects the values of the neighboring pixels.

The ground range data (GRD) product of SENTINEL is usually pre-processed before being released to users. Hence in the SENTINEL image, only calibration and Terrain correction was performed(Veci, 2015). The Radarsat-2 and SENTINEL 1 images were reprojected to the Dutch RD-New coordinate system, EGPS 28992. Afterwards, pixel intensity values were converted into decibel (dB) that stretch brightness range up to -25dB (McNairn & Shang, 2016).

4.5 Visual analysis

To see if there is a relationship between image brightness and presence-absence of shellfish, a visual assessment was performed by superimposing the 2016 shapefiles with shellfish distribution on the SAR Images. This overlay was cross-checked with the field data for presence/absence of shellfish.

4.6 Regression

Regression was applied to assess the relation between shellfish density, and radar backscatter values of each image, whereby the backscatter signal was the independent variable and field data on shellfish density were the dependent variable.

For each plot, RS2C imagery backscatter vas was extracted manually using SNAP toolbox. For a 4 by 4-pixel window around the center of the field plot. This falls within 25m by 25m shellfish bed (see Figure

4-7). The pixel values were extracted and averaged. This averaged value was used in the regression. A similar procedure was done to extract 4-pixel values from the SC1 image with of 2 by 2-pixel window (10m x 10m). The extracted pixel values were averaged to one value to represent each sample plot. The procedure is done for all 50 field plots

4.7 Analysis of Variance (ANOVA)

ANOVA Single Factor was calculated to assess the potential backscatter differences between oyster and mussel species in the Wadden Sea.

4.8 Assess the relation between spatial variability of the backscatter signal and shellfish characteristics

A variogram is a statistic function that is used to determine the variability of a variable with itself. It determines the degree of spatial autocorrelation of paired points that are close to each other. For instance, the variability of shellfish patches in a shellfish bed as shown in Figure 4-15 a). For each field plot, a variogram was plotted as a function of distance for every possible pair of patches between the size and density of shellfish in a shellfish bed. The assumption of this method is that high shellfish density will result in a small range of variation(see Figure 4-16).

4.8.1 Semi-variance Analysis
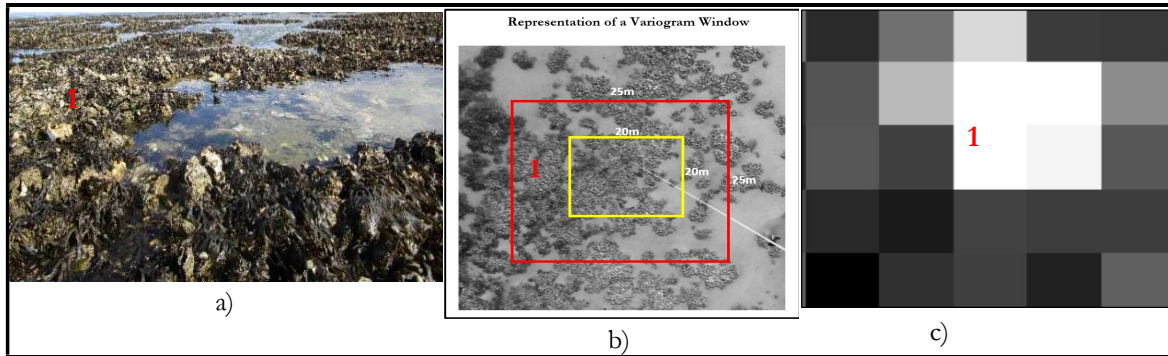
Figure 4-15: a) Field Situation: A representation of mosaic patch of an oyster reef, a representation of a 5 * 5 window obtained from b) aerial photo representing a 20m by 20m of the variogram subset , c)RS2C July Image. **1** indicates the shellfish patch.

Within each field plot, a window of 5x5 pixels from RSC2 July 2017 image, a variogram was plotted. This falls within 25m by 25m shellfish bed (see Figure 4-15 b)and c)). Then using R programming, semi-variance analysis was plotted in the following steps(Bohling, 2005; Choi *et al.,* 2010);

1) Cloud points were displayed to show the spatial autocorrelation of backscatter values to correlate with distance (lag increment) (See Equation 4-2).

$$\hat{y}(d) = \frac{1}{2Nd} \sum_{N(d)} (z(Si) - z(Sj))^2$$

Equation 4-2

Whereby N(d) is set of total pairs in Euclidean distances *d*, *Nd* is the number of pairs in *N(d)*, then *z(si)* and *z(sj)* are data values at spatial scales *si* and *sj*, respectively.

2) Three parameters used were : range (a distance of the differentiation of distant pairs reach a plateau), nugget (discontinuity between the 0 value and where the variogram curve starts) and partial sill that represents variability when there is no spatial correlation.

3) A cutoff of 28 and width of 2m was used as an interval 4m square. This is half of the size of the pixel.

4) It was assumed that the backscatter values are isotropic. This is because rugosity measurement was done both in N-S and W-E with no differences, hence the model is not dependent on the direction of the distance.

5) Spherical and Exponential Models were used to fit variogram obtained points.
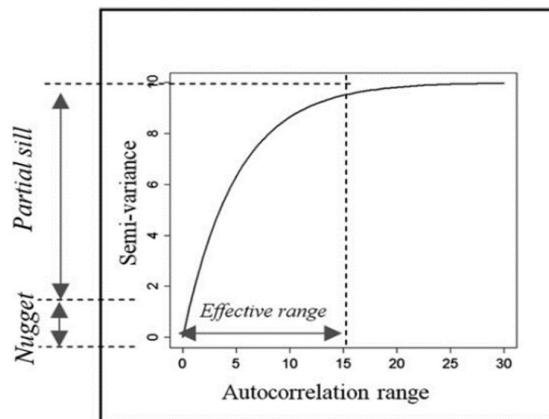
Figure 4-16: Parameters of spherical model of a variogram (Naimi *et al.,* 2011)

4.8.2   Stepwise regression

Pearson correlation was performed to check the collinearity between the sill and range. After that backward regression was performed to fit sill and range with rugosity, shellfish density, and shellfish height. Akaike's 'An Information Criterion' was used determine the best model.

4.9 Mapping

4.9.1   Kriging Interpolation

This is a type of interpolation method that utilizes the spatial structure and variation to predict unsampled areas. Whereby for spatial analysis and classification. In this research, kriging interpolation was applied only to the 2km by 2km subset that had a moderate degree of spatial correlation among the shellfish beds. Cross-validation was performed to test the kriging predictive performance.

4.9.2   Reclassification of Backscatter Values

RSC2 of VV and SC1- HH data was used to determine the distribution of shellfish beds. SC1- HH was collocated to RSC2 –VV. This process also downscales the images from 4m by 4m pixel resolution to 10m by 10m pixel resolution. σ HV. A classified HV map was formed with three classes; shellfish, sediment, and water.

5. RESULTS

5.1 Analysis of field data

A total of 50 observations and measurements were obtained into classes; mussel beds, oyster reefs, mixed shellfish beds and scattered shellfish. For each sample plot the density was determined (i.e., % of the surface covered by shellfish). From the 27 samples in the shellfish beds, the rugosity index and shellfish height were measured. The remaining 23 samples were scattered shellfish and pure sediments.

The Wadden Sea has a varying structure of shellfish beds with different types of sediment. This makes the density of shellfish beds vary among the sample plots (Table 5-1). Although most shellfish beds are mixed, oyster reefs had the highest density and shellfish height as compared to mussel beds. Mixed shellfish beds had a varying contribution of oyster and mussel species. The height of the shells differ between oyster and mussel (see, Appendix 8) where the oyster shells range from 0–12.7 cm and the mussles from 0–3.5 cm.

Table 5-1: Summary statistics of shellfish density , rugosity, and shellfish height field data of 32 sample plots

Value	Oyster (%)	mussel (%)	Mixed shellfish (%)	Scattered shellfish (%)	Shellfish Height(cm)	Rugosity
Minimum value	10	16	35	2	1.6	0.002
First quartile	17.5	20	41	3	2.6	0.008
Median value	35	23	50	5	6.5	0.023
Third quartile	75	61.25	70	7	8.7	0.049
Maximum value	86	81	90	11	12.7	0.533
MEAN	44.63	39.21	57.2	5.6	6.2	0.056
RANGE	76	65	55	9	11.6	0.531
IQR	57.5	41.25	29	4	6.1	0.041

5.2 Visual assessment of the relation between the presence of shellfish beds and the backscatter intensity of the SAR images

In this research Radarsat-2, C band (RSC2) and Sentinel-C band (SC1) were used. Figure 5-1 shows the results of the masked image of a RSC2 mage of the study area . The tidal flats comprise of water and shellfish beds. The zoomed regions show a comparison of RSC2 and SC1 images, having different polarisations in different years. The shapefile overlaps with locations of shellfish. These spots are brighter (high backscatters). However, some other bright areas are associated with wet sand. Darker areas are associated with high moisture/ water levels along the tidal flats. This shows that the SAR signal may be uncertain in different polarisations.
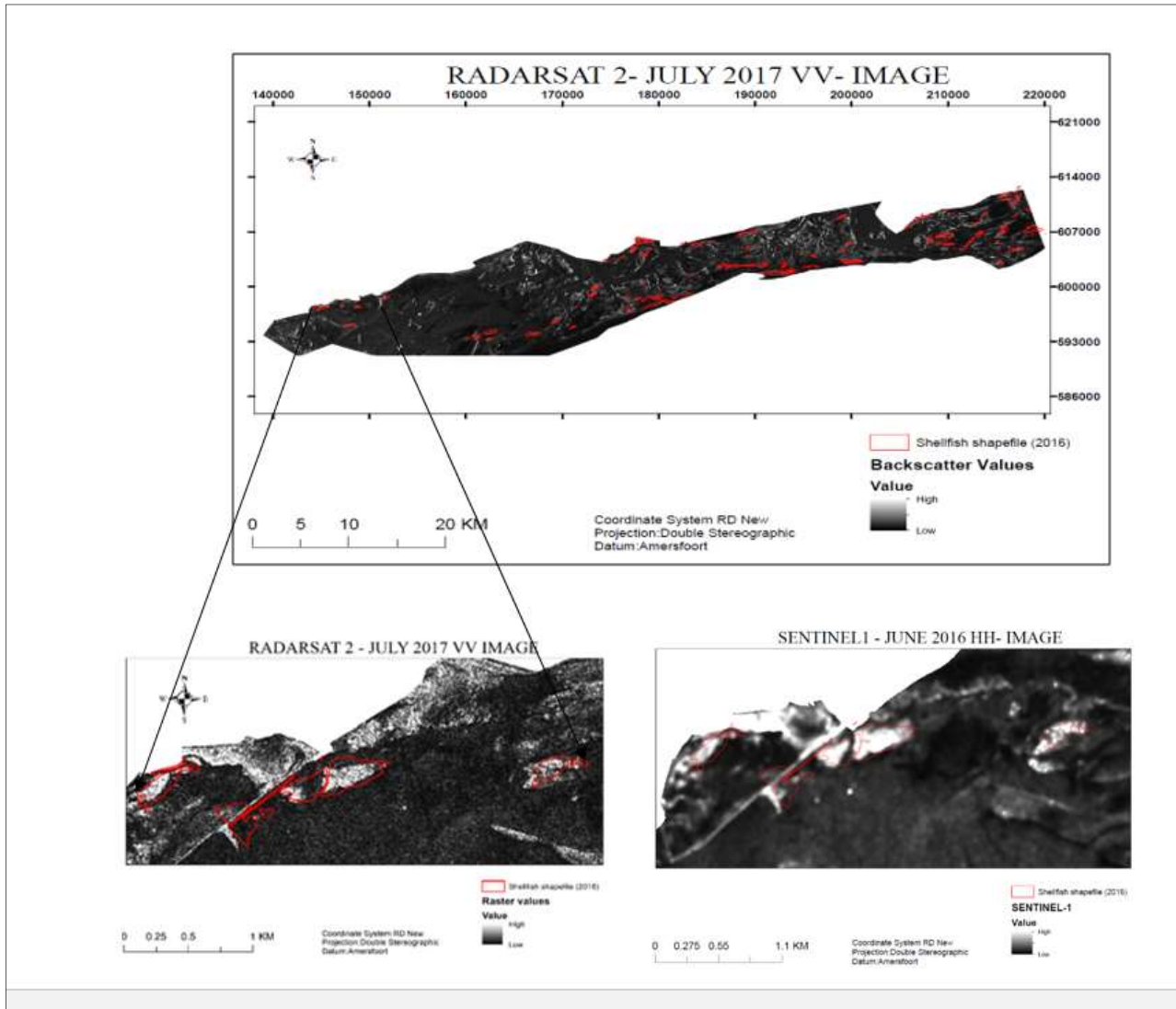
Figure 5-1:Presence of shellfish with SAR signal , RSC2 and SC1 images to a zoomed area near Terschelling island.

5.3 Assess the relation between the density of the shellfish beds and the backscatter signal in different polarisations

Backscatter values were compared using box plots to identify the variation of the signals from one image to another and with different polarisations for all shellfish classes, including bare sediment. Figure 5-2 shows there is a slight difference of variation of backscatter values between the polarisations. HV polarisation extracted from SC1 image shows low backscatter values, regardless of the type of bed coverage. The dB values from mussel and mixed plots vary regardless of the polarisation. In oyster beds, the HV and VV polarisation have an equally significant backscatter as compared to HH polarisations from SC1. There is no polarization where the boxplots of all 5 classes are completely separated.

a)

b)

c)
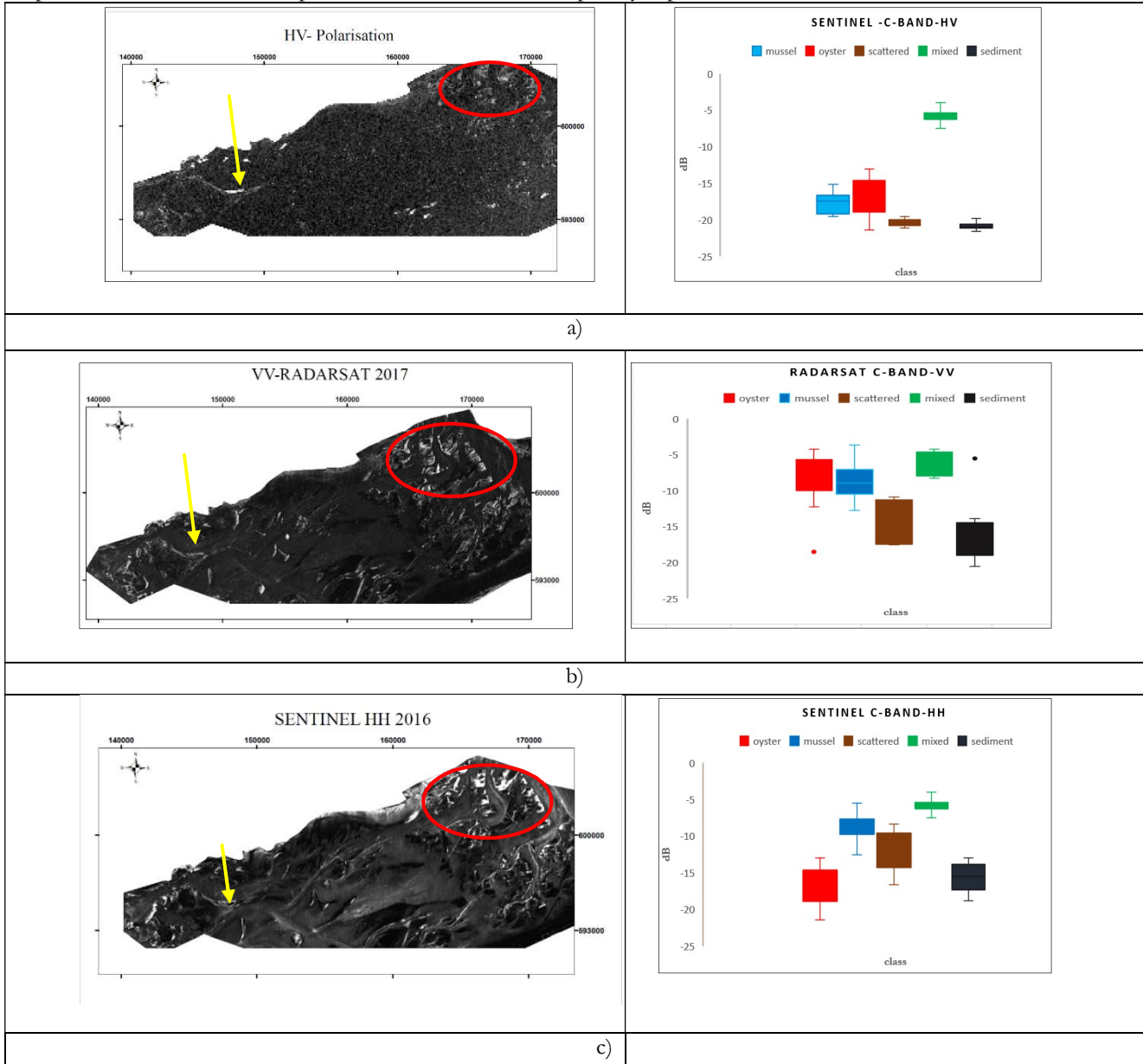
Figure 5-2: Left; SAR images showing : *a)* HV*, b)* VV, and *c)* HH polarisations. Right; boxplots showing the distribution of tidal flats' classes with their dB values. The red circles indicate the locations of sediments, and the yellow arrow indicates a shellfish bed.

In visualization (Figure 5-2), at the red circles(sediment), we see that HV shows low backscatter effect of SAR signal when compared to HH and VV .

Due to the saturation effect, a logarithmic regression was calculated between shellfish density and backscatter values for different polarisations. Logarithmic regression was chosen because it was a good model fit to the dB values and shellfish density than linear regression (See Table 5-2 and Appendix 16) . From the results in Table 5-2, we can see that SC1 HH and RSC2 VV polarised data have R^2 =0.72 respectively with a significance of $p<0.05$ with VV having a low RMSE = 2.3. The two polarised regressed results show the high relationship as compared to HV of $R^2 = 0.59$. Since the regression results of RS2 VV polarized images are nearly the same, it was reasonable to assume that the relation found is due to shellfish density and not to another factor.

Figure 5-3 shows that backscatter values increase as shellfish density increases up to a certain point before leveling off, though this is not observed to HV polarisation. The plateau is a result of saturation point of backscatter values. The estimated saturation point was at -8db with 40% of shellfish density. This effect is a consequence of loss of information at very high backscatter values. Table 5-2 summaries the logarithmic regression results .
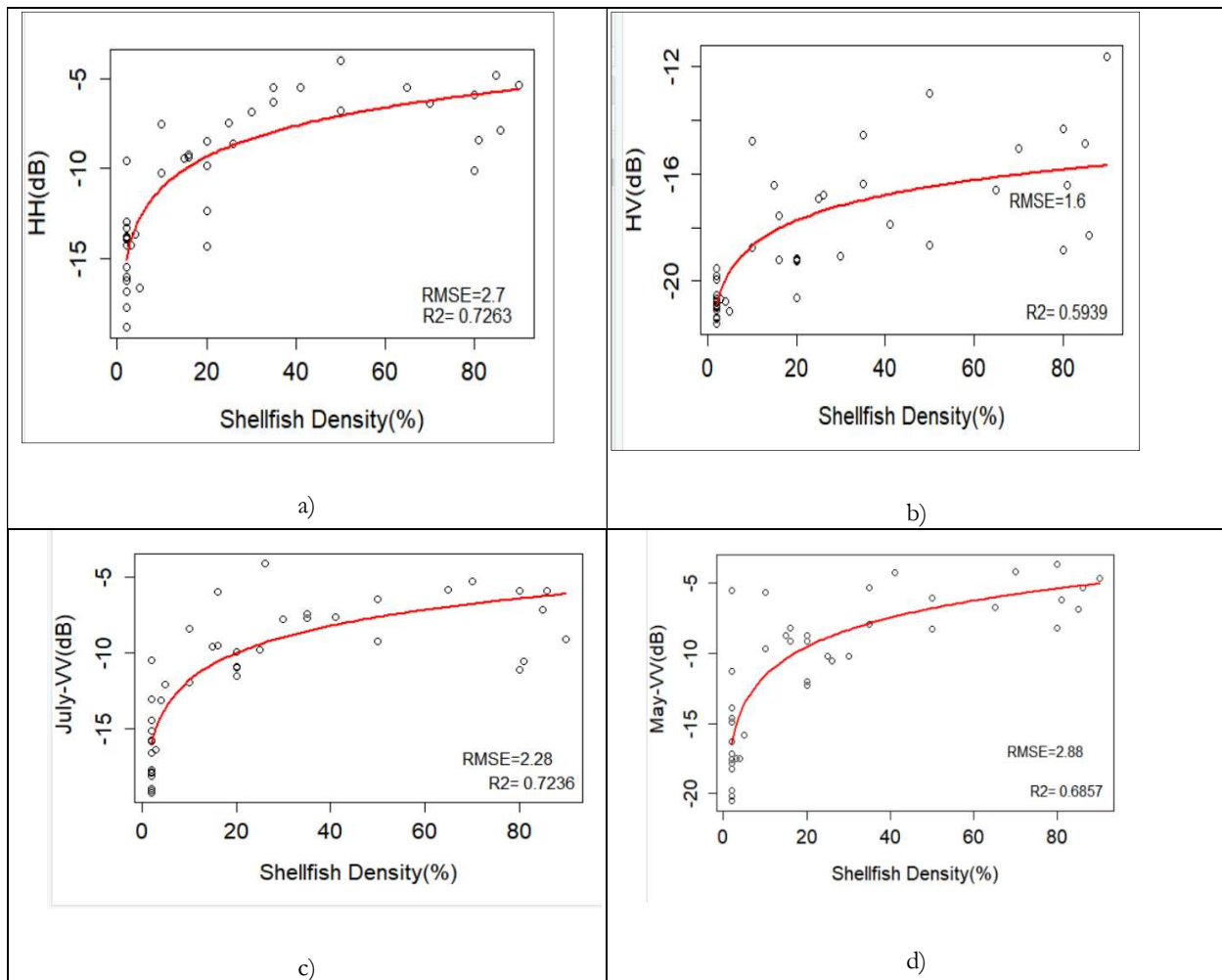
Figure 5-3: Scatterplots of logarithmic regression of different polarized backscatter with shellfish density

Table 5-2. Summary statistics between backscatter values logarithmic regression model of shellfish density per polarization

Backscatter Image	R²	P-Value
14th May 2017- Radarsat VV 18: 21	0.69	8.03e-12
25th July 2017 – Radarsat VV 18:20	0.72	6.007e-13
9th June 2016 - Sentinel HH 18:20	0.72	4.921E-13
9th June 2016 Sentinel HV 18: 20	0.59	1.441e-09

5.4 Asses the relation between the SAR signal with shellfish species

Table 5-3 shows the results obtained from Analysis of Variance (ANOVA), that oyster and mussel species are not significantly different. The F value 0.06 (1,23 df) is less than the F critical value 4.2 at p>0.05. The oyster and mussel species had an equivalent mean of -8dB(σ) with a variance of 17 and 6 respectively and 260 as total variations from the mean. There is no significant relationship of radar backscatter signal with species types.

Table 5-3: ANOVA Single Factor testing the Variation of oyster reefs and mussel beds

Shellfish type	Number of samples	Sum	Average backscatter signal	Variance		
Oyster	11	-93.32	-8.48	17.05		
Mussel	14	-123.73	-8.83	6.85		
Source of Variation	SS	df	MS	F Value	P-value	F critical
Between Groups	0.77	1	0.77	0.068	0.79	4.27
Within Groups	259.62	23	11.28			
Total	260.39	24				

5.5 Assess the relation between spatial variability of the backscatter signal and shellfish characteristics

5.5.1   Semi-variance Analysis

RS2 VV July image was used to calculate semi-variance because SC1 HH image had a pixel size of 10m x 10m allowing a window of only 2x2 pixels to represent a 25m x 25m shellfish bed. This is considered too small for a variogram. Spherical and exponential models were fitted to the experimental variogram results. The spherical model provided a better fit, whereas the exponential model resulted in unrealistic range values as

shown in Appendix 9. Hence spherical model results were used for further statistical analysis. Variogram results had a well-distributed number of paired points (np) per lag distance. Since the nugget obtained was zero (0), the partial sill automatically was used as the sill. Therefore there was no reason for calculating the Signal to Noise Ratio (SNR) as a function to realize the error of each variogram. Appendix 8 shows the summary of spherical variogram analysis of 50 sample plots.

Table 5-4 shows the results of variogram analysis of the 20 sample plots with range and sill parameters. The range obtained from the variogram is equal to the effective range of spatial autocorrelation. The 20 sample plots are the samples that had rugosity index measurement and shellfish height. Generally, the results show that there was no authentic trend in the range within shellfish beds. However, in shellfish beds with high-density, semi-variance signatures reached an optimal sill, while in scattered shellfish and sediment, variogram signatures don't become flat. This automatically shows the spatial variability of the shellfish beds (see Figure 5-4, Figure 5-5, Figure 5-6 and Figure 5-7).

np	dist (m)	semi-variance (γ)
1. 40	2.981324	0.005390090
2. 62	5.061270	0.007335055
3. 48	6.666442	0.007424327
4. 70	9.033605	0.009234175
5. 34	11.095191	0.008008037
6. 36	12.718363	0.004089213
7. 8	14.906618	0.004063717
8. 2	16.864913	0.008233224
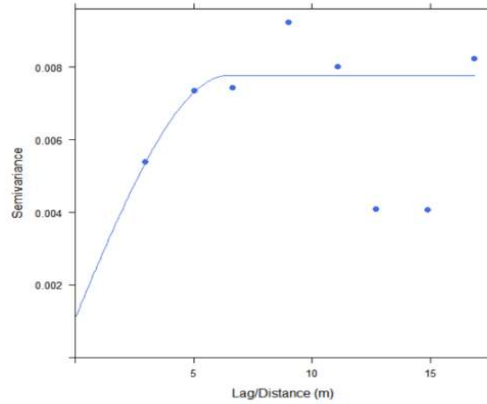
Figure 5-4:Oyster bed - variogram analysis with a range of 6

np	dist (m)	semi-variance (γ)
1. 49	2.981324	2.561805e-04
2. 78	5.067048	5.492827e-04
3. 62	6.666442	7.689475e-04
4. 95	9.038823	8.169805e-
5. 50	11.125628	6.983498e-04
6. 58	12.724862	5.346572e-04
7. 27	14.994087	3.345798e-04
8. 14	16.666070	2.633278e-04
9. 2	19.089785	5.835385e-05
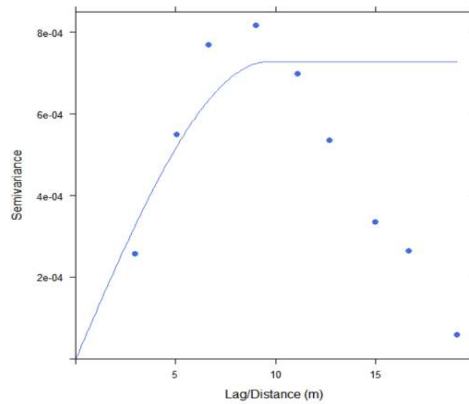
Figure 5-5: Mussel bed – variogram analysis with range of 9m

np	dist (m)	semi-variance(γ)
1. 40	2.981324	0.01046340
2. 62	5.061270	0.02053008
3. 48	6.666442	0.02747872
4. 70	9.033605	0.03433260
5. 34	11.095191	0.04210414
6. 36	12.718363	0.04989349
7. 8	14.906618	0.04733442
8. 2	16.864913	0.04177807
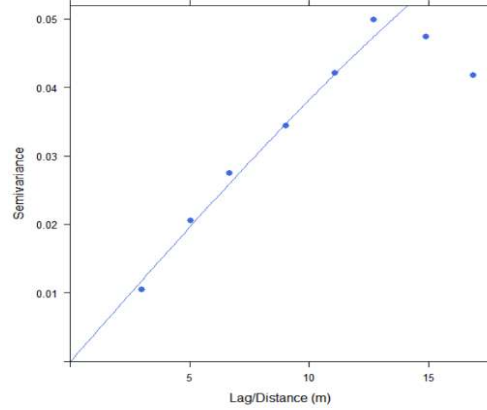
Figure 5-6: Mixed shellfish bed- variogram analysis with a range of 30m

np	dist (m)	semi-variance (γ)
1. 31	2.981324	0.0001412817
2. 46	5.051472	0.0002058861
3. 34	6.666442	0.0001941432
4. 45	9.022590	0.0002697249
5. 18	11.010644	0.0003660414
6. 14	12.691439	0.0003804659
7. 2	14.906618	0.0003975134
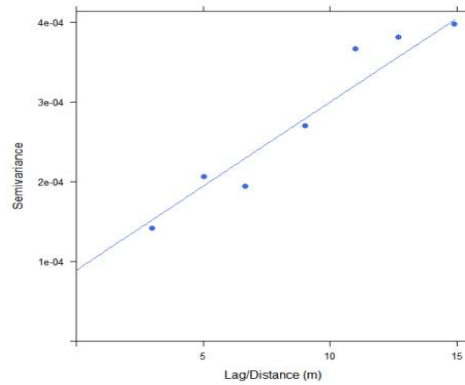
Figure 5-7: Scattered shellfish– variogram analysis with the range of 220m

Table 5-4: Spherical model :Variogram parameters (sill and range) in 20 sample plots

SITE	Range	Sill	Shellfish (%)	Rugosity	Shellfish Height (cm)	Class
B2	9.157643	0.014265	35	0.0575	7.5	mixed shellfish
T1	6.464096	0.134089	41	0.0245	8.6	mixed shellfish
T2	30.63578	0.080845	90	0.043	10.2	mixed shellfish
H1	6.357835	8.37×10^{-5}	20	0.0165	1.6	mussel
H3	7.449525	0.003539	20	0.0085	1.9	mussel
A4	10.7927	0.028892	80	0.005	2	mussel
M1	9.620541	0.000727	45	0.0075	2	mussel
M3	8.265119	0.002261	20	0.0075	2	mussel
H2	7.449525	0.003539	26	0.0215	2.8	mussel
M2	10.19239	0.030905	81	0.011	3.5	mussel
P2	7.856157	1.85×10^{-5}	10	0.0145	5.4	oyster
B1	9.154576	0.003625	50	0.042	6.55	oyster
A2	10.97935	0.000894	30	0.047	7.1	oyster
A1	6.458653	0.006669	85	0.075	8.1	oyster
P1	168.3116	0.127529	86	0.0985	8.8	oyster
T3	19.0202	0.008875	35	0.027	10.7	oyster
B4	13.41899	0.008247	80	0.078	12.4	oyster
P3	83.81619	0.01547	70	0.5325	12.7	oyster
M4	7.038119	0.000311	2	0.002	4	scattered shellfish
A3	7.763618	0.01247	7	0.0075	6.5	scattered shellfish

5.5.2 Stepwise Regression

1. Collinearity and Akaike information criterion

In order to determine the relationship between the characteristics of shellfish beds and the variograms, stepwise regression was performed. The correlation results between variogram parameters (sill and range) show that there is a significant relationship at 95 percent confidence intervals. Variance inflation factor (VIF) results show that there is little collinearity between the two variables. This means that sill and range can be used together as independent variables in the stepwise regression (see Table 5-5).

Table 5-5: Correlation results of sill and range

Pearson's product-moment Correlation	
Df	21
P-Value	0.004
T-Test	3.16
Range	0.2
Sill	0.79
Correlation	0.56
VIF =(Range and Sill)	1.47

2. Backward Regression

To assess the relationship between sill and range on one hand and shellfish bed characteristics, on the other hand, the backward regression was used to identify the best model. AIC criterion was used to counter check the model. Out of the three response variables obtained from the field data, the rugosity index model had a low AIC.

Table 5-6: Best fist models with low Akaike information criterion (AIC)

Variable	Model parameters	AIC
Rugosity	Range , Sill	-252.73
Shellfish density	Range , Sill	330.38
Shellfish Height	Range, Sill	126.7

3. Multiple regression of shellfish characteristics and variogram parameters

The variogram parameters were regressed with the rugosity index , the shellfish height, and shellfish density. The sill and range with rugosity index, shellfish density, and shellfish height show the little relationship (see Table 5-7). Rugosity has a higher significant (p <0.05) relationship of R^2=0.33 with a low standard error as compared to shellfish density with R^2=0.23 and shellfish height with R^2=0.18. This means the variation of SAR signal has a low relationship with field parameters.

Table 5-7: Multiple Regression statistics summary: shellfish density %, shellfish Height(m), Rugosity Index in relation to variogram parameters

Rugosity index with range and Sill		Shellfish Density (%) with Range and Sill		Shellfish Height (cm) with Range and Sill	
Regression Statistics		**Regression Statistics**		**Regression Statistics**	
Multiple R	0.578	Multiple R	0.483	Multiple R	0.432
R Square	0.334	R Square	0.233	R Square	0.186
Adjusted R Square	0.268	Adjusted R Square	0.156	Adjusted R Square	0.105
Standard Error	0.092	Standard Error	26.219	Standard Error	3.802
Observations	23	Observations	23	Observations	23

5.6 Estimating shellfish cover

5.6.1 Reclassification of backscatter values

HV polarized data (a merge of HH – SC1 and VV- RSC2) was used for estimation of shellfish distribution. Shellfish 2016 data (IMARES vector data) had a strong matching relationship with the two-part HV polarized data (see Figure 5-8). The figure shows a reclassified image in ArcGIS with the use of backscatter values. Backscatter values were represented as follows: 23 to -20 dB as water, -20 to -17 dBas sediment and -17 to -6 dB as shellfish beds. The high backscatter values are best aligned with 2016 shellfish cover.
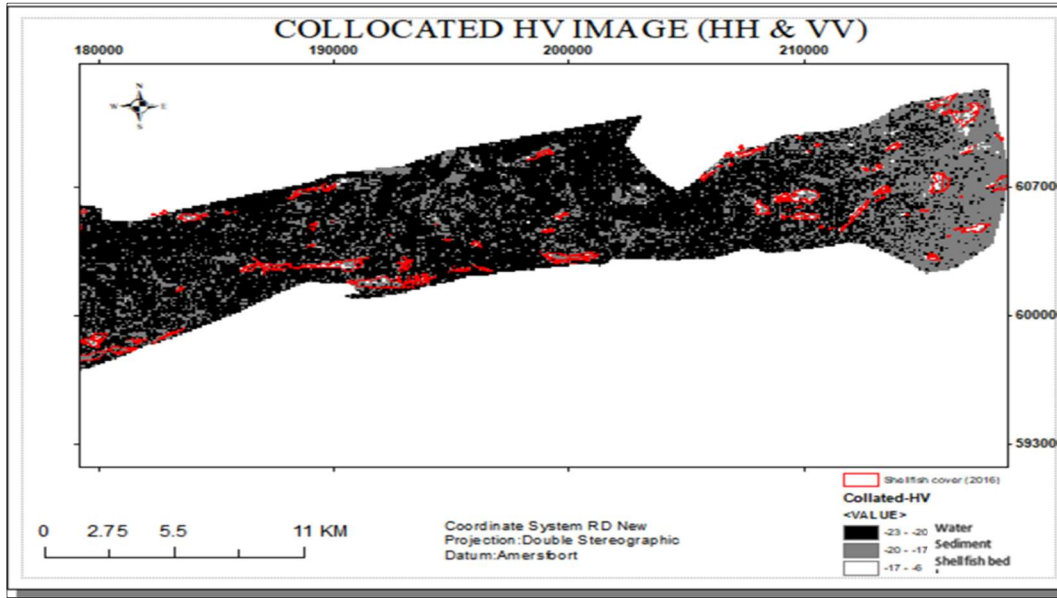
a)
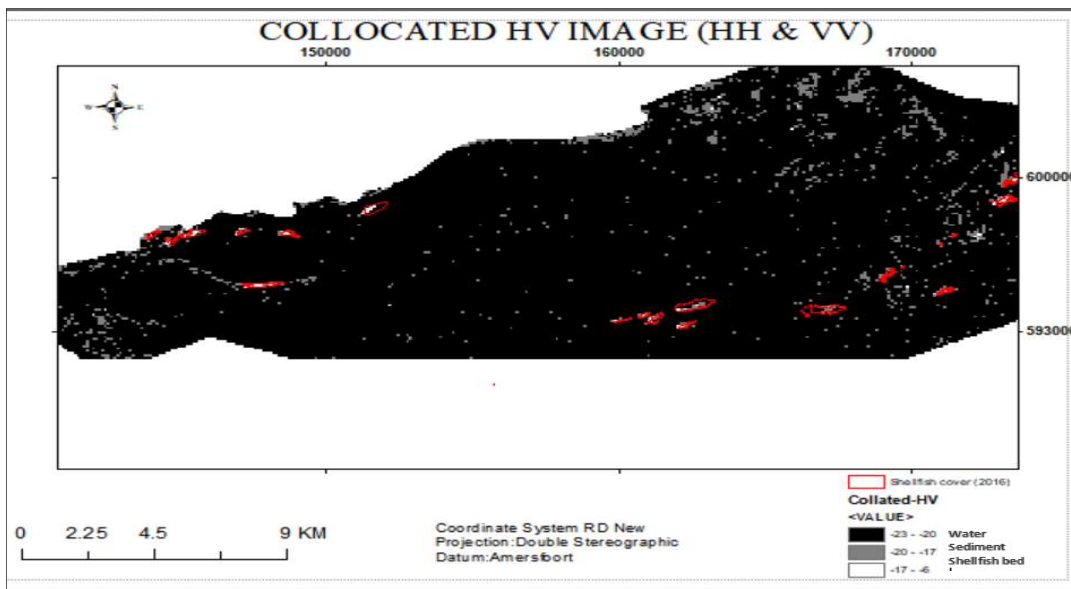
b)

Figure 5-8: HV reclassified image

5.6.2 Kriging Interpolation

To validate the uncertainties of a small subset variogram analysis, a subset of 2km by 2km window was used to determine the variation in different shellfish beds. Exponential variogram was the best fit model with a small SSER(Figure 5-9 c) with its experimental variogram in Figure 5-9 b) demonstrating a convex behavior. The variogram results in Table 5-8 shows 117m range with a nugget of 0.2. This means that 117m was the limit attained to determine the correlation of dB values. The variance of the dB values reached at a sill of 1.6m before forming a plateau distance from the y-intercept (see Figure 5-9 a) and b). Figure 5-9d) shows a directional variogram determining of effects of the dB values in a different direction(anisotropy).

The variograms in Figure 5-9d) move to one direction suggesting that there is a strong spatial autocorrelation with no anisotropy in the tidal flats. Nugget to Sill Ratio (SNR) of 8% was obtained.

Kriging interpolation results in Figure 5-9e show that the spatial pattern of shellfish beds have high dB values (see Figure 5-9f). When compared to shellfish coverage RSC2 SAR image that has superimposed the 2016 IMARES shellfish vector data(see Figure 5-9e), the results show that shellfish beds occupy the relatively small area with backscatter values ranging from -6dB to -17dB when compared with other parts of the tidal flats.

Table 5-8: Summary of Exponential Variogram fit model of a 2km by 2km subset

model	Nugget	Partial sill	Sill	Range	SNR (Sill/Nugget)
Exponential	0.2	1.4	1.6	117.8406	8%

a)

b)

c)

d)
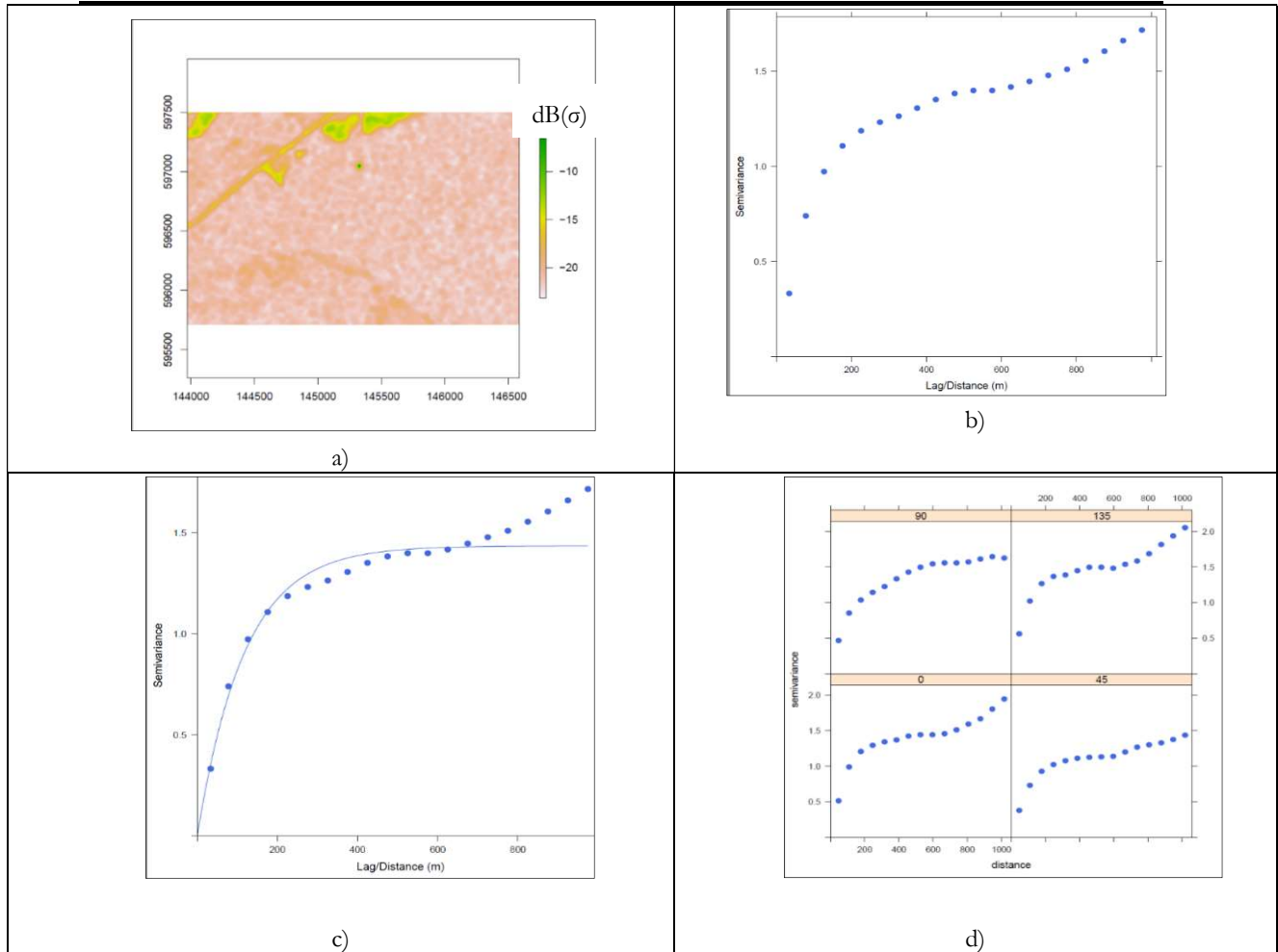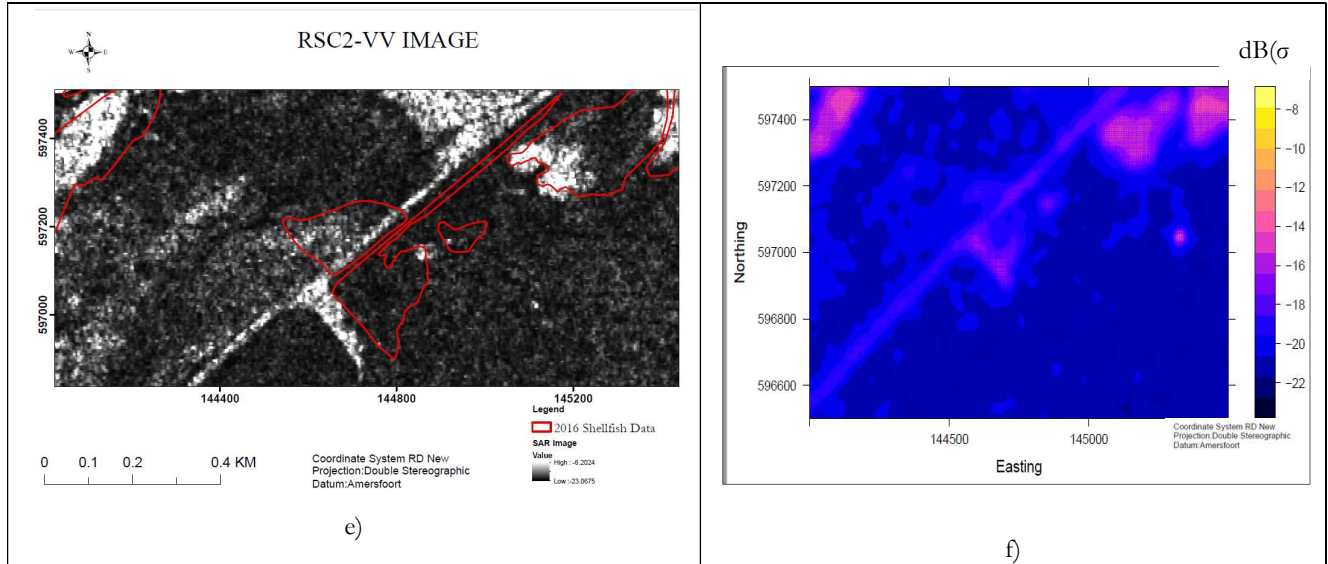
Figure 5-9: a) Subset of the tidal flats b) An experimental variogram of the subset , c) Exponential fit model to the variogram with sill of 1.6 and a range of 117m, d) directional variogram showing there is no anisotropy in the tidal flats, e) the location of shellfish beds when superimposed to the 2016 IMARES shellfish vector data, f) an interpolated scene showing the spatial distribution of shellfish beds.

To estimate the kriging interpolation performance, cross-validation method was used to validate the model. The results in Table 5-9 show an RMSE ≈ 0.9m error.

Table 5-9: RMSE of kriging interpolation of a subset

ME	-0.04
MSE	0.897
RMSE	0.947

5.7. Summary of Results

The results in this chapter indicate that there is a relationship between the presence of shellfish beds and the backscatter intensity of the SAR images. Even with different polarisations, the SAR signal show relationships with shellfish density. However, there is no relationship between the SAR signal with different shellfish species. Also, the spatial variability of the backscatter signal and shellfish characteristics cannot be distinguished in a single shellfish bed. The next chapter, therefore, moves on to discuss the results with respect to research questions.

6. DISCUSSION

6.1 Visual assessment of the relation between the presence of shellfish beds and the backscatter intensity of the SAR images

The 27 samples in the tidal flats have a variation of shellfish density and species composition. The range between the oyster reefs and mussel bed density is 76% and 65% respectively suggesting that oyster reefs have a denser cover as compared to mussel beds. This finding is consistent with Troost (2009) who argued that an increase in oyster density was as a result of its successful trait to be able to invade and adapt to environmental conditions thus it being able to spread rapidly on the tidal flats.

Another important finding was that the mixed shellfish beds have a varying contribution of oyster and mussel species. Observed uneven combination increases the shell height variation and in return causing a high backscattering effect of the SAR signal. As a consequence, high backscatter values occurred in mixed beds. Similar findings have been reported by Nieuwhof *et al.,* (2015) with use of LiDAR point cloud data.

When we superimposed the 2016 IMARES shellfish vector data to Radarsat-2 C band (RSC2) VV image, it confirmed that bright areas are associated with shellfish density (see Figure 5-1). The bright areas are the result of high backscatter (dB) values onto which are attributed to the structure caused by high shellfish density. Increase in shellfish density cause increase in backscattering thus resulting to high dB values (Wang *et al.*, 2017).

However, there are other bright areas associated with more sandy sediments. A possible explanation for this might be that the false positive brightness areas observed are mostly situated along the edges of dry fallen sand flats and edges of creeks. Sand flats are composed of sandy ripple heights (Wang *et a.,* 2017) due to layover effects of the SAR signal of the radar look direction and incidence angle. When the SAR signal senses the highest point of a surface before the surrounding image, it makes the highest points have brighter backscatter effects than the surroundings (Melchionna & Gade 2014).

An additional important observation was that darker areas are associated with water content, meaning that the areas have low dB values. Water channels such as creeks and water pools have a smooth surface resulting to specular reflection thus causing low backscatter values (Kim *et al.,* 2011). However, White *et al.,* (2015) argued that only calm water results in low backscatter. At high tide levels, high rough waves will cause an effect which increases the dB values. Hence tidal level information must be taken into consideration when acquiring SAR images.

Different types of sediments show different backscatter effects with the SAR signal. Mudflat regions had low dB values, then followed by wet sandy areas (higher content of water), sand flats have high dB values, with the highest being -7dB, roughness decreased with the increasing content of mud (see Appendix 5). A possible explanation is that SAR backscatter was affected by a physical characteristics such as grain size, porosity behavior under tidal currents and moisture content in the soil (Deroin, 2012). Sand has large grain-size as compared to mud. The SAR signal scatters from different sand grain sizes causing a signal interaction between the sand particles (Gade *et al.*, 2014). Also, micro-relief in sediments such as sand ripples and sandworms, resulting in an increase of surface scattering causing high dB values (van der Wal & Herman 2007).

6.2 Assess the relation between the density of the shellfish beds and the backscatter signal in different polarisations

Logarithmic regression showed that there was a significant relationship between shellfish density and backscatter (dB) values in VV and HH. The RSC2 VV July image was taken at lower tide as compared to the one taken in May. However , there is a high relationship between these images considering that both regressions have a coefficient of 0.95 as shown in Appendix 6. Also, the two regression results of RS2 VV are nearly the same. Hence it is reasonable to assume that the relation found is due to shellfish density and not to another factor.

Logarithmic regression was used to relate shellfish density and dB values because the model fitted with the distribution of related variables. Similar observations of logarithmic regression results were also made by Nga (2010) and Chandola (2014) in biomass estimation and (Nieuwhof *et al.,* (2015) in shellfish detection. In these latter studies, logarithmic regression was chosen because of the SAR signals saturation characteristics affected by surface variation. The saturation is due to the fact that incoming SAR signals hit different parts of the nonuniform surface, then as they return back to the sensor, they interact with new incoming SAR signals causing more absorption resulting to saturation effect(McNairn & Shang, 2016).

Even though there is a significant relationship between the shellfish density and the SAR signal, we observed that it was difficult to differentiate scattered shellfish (<10% shellfish density) from sediment in SAR signal (see Appendix 7). Hence it would be difficult to monitor shellfish density in juvenile stages and in a new area.

It is interesting to note that VV and HH polarisations had a stronger significant (R^2=0.72, p=<0.05) relationship to shellfish density compared to HV polarisation.(R^2=0.59, p=<0.05) (see Table 5-2). HH and VV have characteristics of high surface scattering when compared to HV because a higher percentage of SAR signal energy is sent back to the sensor. The results support the findings of Gade *et al.* (2014) whereby HH polarisation was able to discriminate water and land. They recorded that water is less scattering because of its less sensitivity to capillary waves.

Even though the VV and HH have similar regression results, VV has been reported to have a disadvantage in surface scattering when compared to HH. Vertically polarized waves tend to lose the scattering efficiency much faster as compared to horizontally polarized waves. Secondly, shellfish beds are vertically aligned which increases the absorption of vertically transmitted waves, thus reducing backscattering effect of VV when compared to HH . Hence HH polarisation is recommended for determining characteristics of a surface (Gade *et al.,* 2014).

The low regression results observed in HV (cross) polarisation is due to the effect of high absorption of SAR signal onto the surface, resulting in less energy being returned to the sensor. Hence it causes volume scattering to exposed penetrative objectives, resulting in low dB values in the tidal flats (Choe *et al.,* 2012 ; Ban, 2016). However, in visualization, it could be seen that HV shows low backscatter effect of the SAR signal when compared to HH and VV due to volume scattering, hence an important aspect in cross polarisation.

6.3 Asses the relation between the SAR signal with shellfish species

Analysis of variance (ANOVA) results shows that oyster and mussel species are not significantly different. The observed relationship between shellfish density and dB values might be explained as follows: -

1. Mixed shellfish beds

Most shellfish beds are of mixed species. Hence it becomes a challenge to determine the range of dB values from one shellfish species to another. For instance, backscatter values of oyster species varied from -20 to -12 while mussel species varies from -16 to -19 in HV polarisation. In VV polarisation oyster species varies between -4 to -12 while mussel species varies from –3 to -12 (see Appendix 4).

2. Wavelength type

C- band wavelength used in this research is a longer wavelength than X-band. Hence it weakens the backscattering effect resulting in similar dB values for oysters and mussels. Similar results were observed with Choe *et al.* (2012) when they used much L band wavelength , a much longer wavelength to the C. band. However, findings from Wang *et al.* (2017) show that the X-band sensor is able to show a higher roughness scale in oyster reefs than in mussel beds. Hence in future investigations, it might be possible to use X band images.

3. Saturation effect

Backscatter intensity saturates at approximately 40% shellfish density in shellfish beds. These findings suggest that it is difficult to extract information on shellfish beds or species composition (Nieuwhof *et al.* (2015). In order to reduce the effect of saturation, Choe *et al.* (2012) advised the use of low incidence angles that may reduce the attenuation effect (high absorption).

4. Species overlap

Box plots of oysters and mussels in HV and VV overlap meaning that it is difficult to distinguish between species. HV is good in volume scattering hence able to differentiate the mixed beds. Boxplots in HH, on the other hand, distinguish the only oyster from the other classes but difficult to distinguish between scattered shellfish from the mussel beds. This is because HH polarisation has a high surface scattering effect than VV. The scattered shellfish are usually mostly oyster shells that also increase the surface scattering.

6.4 Assess the relation between spatial variability of the backscatter signal and shellfish characteristics

Some sample plots such as scattered shellfish and sediments have a larger range of spatial autocorrelation than the diagonal length of the subset. (see Appendix 8). These results suggest that the np (number of pairs) points are not correlated hence receiving little weight when predicted by the variogram model. Jensen (2004) and Troost (2009) help us understand that each visited site is unique with varied shellfish patches and water pools (see Figure 4-7). The distance between patches and shapes of an object may vary from one shellfish bed to another. As a result, the varied shellfish patches show different variation resulting in different scales of autocorrelation (Kelly *et al.*,2003; Morris, 2005).

Other factors that may have contributed to the low relationship of variogram parameters with field data are:
1. **Rugosity Index measurement**

The was a low significant relationship between the characteristics of shellfish beds and the variogram parameters. (see Table 5-7). The high density is due to compaction of shellfish together forming a 'blanket' of biomass. This 'blanket' makes the chain for rugosity measurement to be longer since it does not accurately follow the surface roughness, thus showing the same results when compared to a sparsely scattered shellfish bed. Rugosity index using a chain may not be an appropriate indicator for determining surface roughness of shellfish beds. However, Choe *et al.* (2012) showed that the IEM model parameters demonstrated a clear variation of shellfish bed up to 1m variation shellfish on a patched shellfish bed (see Figure 6-1).
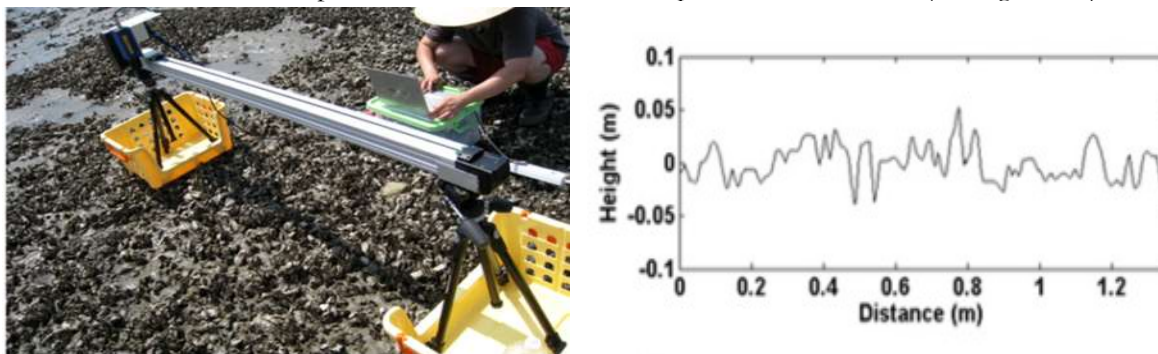
Figure 6-1: Surface roughness measurement with the use of laser surface profiler (Choe *et al.*, 2012)

2. **The size of the subset window**

Tonye *et al.* (2011) argued that different window sizes lead to different results, so an appropriate window size for variogram analysis is necessary. In this study, a 5 x 5-pixel window was reasonably small in variogram analysis to the extent that 90% of the variograms analyzed had a Nugget of zero (0). Hence Sill to Nugget ratio (SNR) was not calculated. The SNR is an important factor to determine the nugget error away from the intercept. Similar findings from Wu *et al.* (2006) show that small window is not effective in analyzing the spatial relationship of different covers. A possible explanation for this might be that the number of pairs (np) is reduced hence not able to characterize the behavior of the variogram. However, when the window is too large, it conflicts with neighboring pixels resulting in a variance of a mixture of different textures from the subset. Hence Tonye *et al.* (2011) opted to add fractal model (slope) to variogram parameters when classifying urban areas.

6.5 Estimating shellfish cover

The estimated results of reclassification and kriging interpolation show that the shellfish species can be discriminated from the surroundings. As stated by Tobler's first law of geography, the closer objects are to each other, the more they are related rather than to distant objects. Hence, the spatial dependence of shellfish roughness is within a single bed. Cross validation test showed an RMSE ≈ 0.9m in the prediction of shellfish beds allowing us to see the spatial variability of shellfish beds. Location of small patches with high dB values in Figure 5-9 e) corresponded with the 2016 IMARES vector data. It is quite evident that the density of

shellfish beds varies from one bed to another. As mentioned by Troost (2009), the spatial variation of shellfish beds may partly be explained by the availability of food and high phenotypic variation.

SNR represents a spatial heterogeneity caused by total spatial variation in an area. Using Lu and Liu (2012) criteria (SNR < 25 % ~high , =50 %~moderated, > 75 %~ low), the SNR value was less than 25% indicating that the spatial heterogeneity in the dB values is low. This suggests that the variogram model has a strong spatial correlation.

Table 6-1 summarizes the estimated shellfish beds using the two techniques .The kriged interpolated results had much clear density variation as compared to the reclassified HV image . This suggests that the increase of shellfish density results in an increase in backscatter when compared to IMARES data overlayed in Figure 5-8. Even though, there was no accuracy assesment performed ,the IMARES polygon showed a larger area covered by shellfish beds as compared to the kriged SAR image. The reason for this is not clear , but it may have something to do with shellfish beds having no clear boundaries, hence increasing the uncertainity of shellfish coverage (Nieuwhof *et al.,* 2015).

Table 6-1: Summary of estimated dB values of shellfish beds

Maps	Estimated dB values of shellfish beds
Reclassified HV image	-17 to -6
Kriging interpolation results	-14 to -6

6.6 Research relevance to management of tidal flats

Tidal flats are highly productive ecosystems. To manage the inaccessible parts of coastal zones, SAR signal independent of weather can be collected any time of the day and night. TERRASAR-X satellite band (not freely available) promotes a high surface scattering as compared to Sentinel 1 –C band (which is freely available). To estimate the shellfish beds and their distribution in the tidal flats, kriging interpolation shows a clear estimate of shellfish distribution in the tidal flats. Quantitative maps of shellfish beds will allow TMAP to potentially monitor tidal flats.

7. CONCLUSION AND RECOMMENDATIONS

6.1 Conclusion

This study tested the discrimination shellfish beds with surrounding using SAR image of Dutch Wadden Sea. Shellfish beds can be detected with the use of C-bands of SENTINEL -1 and RASARSAT-2 data. Tidal flats have different spatial structures. These structures respond differently with various polarizations. The spatial distribution pattern of shellfish beds was attained by applying kriging interpolation method in R programming and reclassification from ArcGIS software. For each objective, a conclusion is as follows:

1. **Assess the characteristics of polarization of SAR backscatter from shellfish beds with different densities and species composition in relation to the surrounding tidal flats**

    Is the backscatter signal of SAR image associated with the presence of shellfish beds?

The presence of shellfish beds correlated with radar backscatter values. Hence there is a different SAR signal in different polarisations with shellfish beds and their surroundings. Shellfish bed areas had higher backscatter values as compared to sediments and other wet areas. A low tide (no rough waves) is the main criterion for acquiring images for analysis.

    Is the backscatter signal of SAR image associated with density of shellfish beds?

    H_0: There is no significant difference in the radar backscatter signal of different polarisations with shellfish densities.

There is a significant relation between the radar backscatter signal of different polarisations and shellfish densities. VV and HH polarized data had a high relationship of 72% in detecting the shellfish beds. In essence, the relationship between backscatter and shellfish beds followed an optimum rather than linear curve due to saturation. Hence maximum backscatter values were observed to reach a plateau when correlated with shellfish density. In conclusion, the null hypothesis is rejected.

    Is the backscatter signal of SAR image associated with species composition of shellfish beds?

    H_0: There is no significant difference in the radar backscatter signal with species composition.

ANOVA results show no variation of dB related to species. Hence the null hypothesis cannot be rejected.

    Is the backscatter signal variation associated with shellfish density and surface roughness (rugosity and height)?

    H_0: There is no significant relation between backscatter signal variation with shellfish density and surface roughness (rugosity and height).

There is a weak relationship between backscatter values variation with a surface roughness (rugosity and height). There is a weak degree of spatial autocorrelation within a shellfish bed. Sill and range of spatial correlation in backscatter varied within the beds resulting in a different range of variations. However, there is a strong degree of spatial autocorrelation from a large spatial scale from one shellfish bed to another. In conclusion, the null hypothesis cannot be rejected.

2. Map the spatial distribution and density of shellfish beds at species level with SAR imagery

How accurate can SAR data Map shellfish beds distribution and density? How accurate can SAR data Map shellfish beds distribution and species composition?

There was no accuracy performed since the field data were few, however, the cross-validated results from Kriging interpolation showed that there is a spatial distribution pattern of shellfish beds due to the fact that shellfish beds, in general, have a high backscatter signal than the surrounding sediments and water. The backscatter values of shellfish class also correspond to a certain extent with 2016 shellfish bed vector map.

6.2 Recommendation

The following studies would improve the outcome of this research;

1. Roughness field measurement should be taken using the laser profiler or a pin-point table method instead of a chain, in order to better capture surface roughness. show a spatial variation of shellfish beds.
2. Alternatively, LIDAR data should be incorporated to provide shellfish height information.
3. The use of high-resolution images would increase the variogram analysis window. This would assist in determining the nugget variance with a range from each bed, thus show the best variation in density.
4. Furthermore, kriging interpolation may determine the spatial distribution pattern of the tidal flats or rather use fractal dimension calculations.
5. Further research should focus on using X band wavelength on the tidal flats to show the differences. This is because X band is a shorter wavelength with higher power to support detection of smaller objects.

LIST OF REFERENCES

Adolph, W., Schückel, U., Son, C. S., Jung, R., Bartholomä, A., Ehlers, M., … Farke, H. (2017). Monitoring spatiotemporal trends in intertidal bedforms of the German Wadden Sea in 2009–2015 with TerraSAR-X, including links with sediments and benthic macrofauna. *Geo-Marine Letters*, *37*, 79–91. https://doi.org/10.1007/s00367-016-0478-y

Bohling, G. (2005). Introduction to Geostatistics and Variogram Analysis. Retrieved from http://people.ku.edu/~gbohling/cpe940

Brockmann, C., & Stelzer, K. (2008). Optical Remote Sensing of Intertidal Flats. In Barale & Gade (Eds.), *Remote Sensing of the European Seas* (pp. 117–128). Springer Netherlands. https://doi.org/10.1007/978-1-4020-6772-3_9

Chandola, S. (2014). *Polarimetric SAR Interferometry for Forest Aboveground Biomass Estimation- MSc Thesis*. University of Twente. unpublished.

Choe, B. H., Kim, D. jin, Hwang, J. H., Oh, Y., & Moon, W. M. (2012). Detection of oyster habitat in tidal flats using multi-frequency polarimetric SAR data. *Estuarine, Coastal and Shelf Science*, *97*, 28–37. https://doi.org/10.1016/j.ecss.2011.11.007

Choi, S.-B., Kang, C.-W., & Cho, J.-S. (2010). Data-Dependent Choice of Optimal Number of Lags in Variogram Estimation. *The Korean Journal of Applied Statistics*, *23*(3), 609–619. https://doi.org/10.5351/KJAS.2010.23.3.609

Colwell, M. A. (2010). *Shorebird ecology, conservation, and management*. California: University of California Press.

Common Wadden Sea Secretariat. (2008). TMAP guidelines for an integrated Wadden Sea monitoring. Wilhelmshaven, Germany. Retrieved from www.waddensea-secretariat.org

Cooley, P. M., & Barber, D. G. (2003). Remote Sensing of the Coastal Zone of Tropical Lakes Using Synthetic Aperture Radar and Optical Data. *Journal of Great Lakes Research*, *29*, 62–75. https://doi.org/10.1016/S0380-1330(03)70539-5

Dankers, N., Brinkman, A. G., Meijboom, A., & Dijkman, E. (2001). Recovery of intertidal mussel beds in the Waddensea: Use of habitat maps in the management of the fishery. *Hydrobiologia*, *465*, 21–30. https://doi.org/10.1023/A:1014592808410

Dankers, N., van Duin, W., Baptist, M., Dijkman, E., & Cremer, J. (2012). The Wadden Sea in the Netherlands: Ecotopes in a World Heritage Barrier Island System. In P. T. Harris & E. K. Baker (Eds.), *Seafloor Geomorphology as Benthic Habitat* (1st ed., pp. 213–226). Waltham: Elsevier Inc. https://doi.org/10.1016/B978-0-12-385140-6.00011-6

Daskalov, G. M., Grishin, A. N., Rodionov, S., & Mihneva, V. (2007). Trophic cascades triggered by overfishing reveal possible mechanisms of ecosystem regime shifts. In S. R. Carpenter (Ed.), *PNAS* (Vol. 104, pp. 10518–10523). PNAS. https://doi.org/https://doi.org/10.1073/pnas.0701100104

Davaasuuren, N., Stapel, J., & Dankers, N. (2014). *Satellite Data :Overview of satellite data for long term monitoring in the wadden sea ,WALTER*. Wageningen: IMARES Wageningen UR. Retrieved from http://www.walterwaddenmonitor.org/wp-content/uploads/Overview-of-satellite-data-for-long-term-monitoring-in-the-Wadden-Sea-WaLTER.pdf

Deroin, J. P. (2012). Combining ALOS and ERS-2 SAR data for the characterization of tidal flats. Case study from the Baie des Veys, Normandy, France. *International Journal of Applied Earth Observation and Geoinformation*, *18*(1), 183–194. https://doi.org/10.1016/j.jag.2012.01.019

Durden, S. L., van Zyl, J. J., & Zebker, H. A. (1989). Modeling and observation of the radar polarization signature of forested areas. *IEEE Transactions on Geoscience and Remote Sensing*, *27*(3), 290–301. https://doi.org/10.1109/36.17670

Ens, B. J. (2003). What we know and what we should know about mollusc fisheries and aquacultures in the Wadden Sea. In W. J. Wolff, K. Essink, A. Kellerman, & A. van Leeuwe M (Eds.), *Proceedings of the 10th International Scientific Wadden Sea Symposium, 2000*. Den Haag.: Ministerie van LNV.

Ens, B. J. (2006). The conflict between shellfisheries and migratory waterbirds in the Dutch Wadden Sea. In G. C. Boere, C. A. Galbraith, & D. A. Stroud (Eds.), *Waterbirds around the world* (1st ed., pp. 806–811). Edinburgh: The Stationery Office.

Eriksson, B. K., Van Der Heide, T., Van De Koppel, J., Piersma, T., Van Der Veer, H. W., & Olff, H. (2010). Major Changes in the Ecology of the Wadden Sea: Human Impacts, Ecosystem Engineering and Sediment Dynamics. *Ecosystems*, *13*. https://doi.org/10.1007/s10021-010-9352-3

ESA. (2017). ERS Radar Courses - ESA Operational EO Missions - Earth Online. Retrieved August 20, 2017, from https://earth.esa.int/web/guest/missions/esa-operational-eo-missions/ers/instruments/sar/applications/radar-courses/content-3/-/asset_publisher/mQ9R7ZVkKg5P/content/radar-course-3-synthetic-aperture-radar

ESA Earth Online. (2017). Sentinel-1 - ESA EO Missions - Earth Online - ESA. Retrieved August 6, 2017, from https://earth.esa.int/web/guest/missions/esa-operational-eo-missions/sentinel-1

Fey, F., Dankers, N., Meijboom, A., De Jong, M., Van Leeuwen, P., Dijkman, E., & Cremer, J. (2007). *De ontwikkeling van de Japanse oester in de Nederlandse Waddenzee : Situatie 2006. Wageningen IMARES*.

Folmer, E. O., Drent, J., Troost, K., Büttger, H., Dankers, N., Jansen, J., … Philippart, C. J. M. (2014). Large-Scale Spatial Dynamics of Intertidal Mussel (Mytilus edulis L.) Bed Coverage in the German and Dutch Wadden Sea. *Ecosystems*, *17*(3), 550–566. https://doi.org/10.1007/s10021-013-9742-4

Gade, M., Alpers, W., Melsheimer, C., & Tanck, G. (2008). Classification of sediments on exposed tidal flats in the German Bight using multi-frequency radar data. *Remote Sensing of Environment*, *112*(4), 1603–1613. https://doi.org/10.1016/j.rse.2007.08.015

Gade, M., Kohlus, J., & Kost, C. (2017). SAR Imaging of Archaeological Sites on Intertidal Flats in the German Wadden Sea. *Geosciences*, *7*(4), 105. https://doi.org/10.3390/geosciences7040105

Gade, M., & Melchionna, S. (2016). Joint use of multiple Synthetic Aperture Radar imagery for the detection of bivalve beds and morphological changes on intertidal flats. *Estuarine, Coastal and Shelf Science*, *171*(January), 1–10. https://doi.org/10.1016/j.ecss.2016.01.025

Gade, M., Melchionna, S., Stelzer, K., & Kohlus, J. (2014). Multi-frequency SAR data help improving the monitoring of intertidal flats on the German North Sea coast. *Estuarine, Coastal and Shelf Science*, *140*, 32–42. https://doi.org/10.1016/j.ecss.2014.01.007

Gade, M., Stelzer, K., & Kohlhus, J. (2010). Long-Term Remote Sensing of the Wadden Sea Ecosystem on the German North Sea Coast. In *Proceedings of ESA Living Planet Symposium, held on 28 June - 2 July 2010*. Bergen , Norway. Retrieved from https://www.researchgate.net/profile/Martin_Gade2/publication/262522484_Long-

Term_Remote_Sensing_of_the_Wadden_Sea_Ecosystem_on_the_German_North_Sea_Coast/links/5
68d35c808aeaa1481ae408b.pdf

Goodman, J. W. (1976). Some fundamental properties of speckle. *Journal of the Optical Society of America*, *66*(11), 1145. https://doi.org/10.1364/JOSA.66.001145

Grizzle, R. E., Adams, J. R., & Walters, L. J. (2002). Historical changes in intertidal oyster (Crassostrea virginica) reefs in a Florida lagoon potentially related to boating activities. *Journal of Shellfish Research*, *21*(2), 749–756. https://doi.org/10.2983/035.029.0302

Harris, P. T., & Baker, E. K. (2012). Why Map Benthic Habitats? In P. T. Harris & E. K. Baker (Eds.), *Seafloor Geomorphology as Benthic Habitat* (1st ed., pp. 3–22). Waltham: Elsevier Inc. https://doi.org/10.1016/B978-0-12-385140-6.00001-3

Horstmann, J., & Koch, W. (2008). High Resolution Wind Field Retrieval from Synthetic Aperture Radar: North Sea Examples. In V. Barale & M. Gade (Eds.), *Remote sensing of the European seas* (1st ed.). Dordrecht: Springer. https://doi.org/https://doi.org/10.1007/978-1-4020-6772-3_25

Jensen, O. P. (2004). *Spatial Ecology of Blue crab (Callinectes Sapidus) in Chesapeake Bay (MSc Thesis)*. University of Maryland.

Jung, R., Adolph, W., Ehlers, M., & Farke, H. (2015). A multi-sensor approach for detecting the different land covers of tidal flats in the German Wadden Sea — A case study at Norderney. *Remote Sensing of Environment*, *170*, 188–202. https://doi.org/10.1016/j.rse.2015.09.018

Kim, D., Moon, W. M., Kim, G., Park, S.-E., & Lee, H. (2011). Submarine groundwater discharge in tidal flats revealed by space-borne synthetic aperture radar. *Remote Sensing of Environment*, *115*(2), 793–800. https://doi.org/10.1016/j.rse.2010.11.009

Klemas, V. V. (2014). Advances in coastal wetland remote sensing. In *Measuring and Modeling of Multi-Scale Interactions in the Marine Environment - IEEE/OES Baltic International Symposium*. Tallinn: IEEE. https://doi.org/10.1109/BALTIC.2014.6887873

Koch, M., Schmid, T., Reyes, M., & Gumuzzio, J. (2012). Evaluating full polarimetric C- and L-band data for mapping wetland conditions in a semi-arid environment in central Spain. *IEEE Journal of Selected Topics in Applied Earth Observations and Remote Sensing*, *5*(3), 1033–1044. https://doi.org/10.1109/JSTARS.2012.2202091

Lee, Y. K., Park, J. W., Choi, J. K., Oh, Y., & Won, J. S. (2012). Potential uses of TerraSAR-X for mapping herbaceous halophytes over salt marsh and tidal flats. *Estuarine, Coastal and Shelf Science*, *115*, 366–376. https://doi.org/10.1016/j.ecss.2012.10.003

Lee, J. Sen, Grunes, M. R., & Grandi, G. de. (1999). Polarimetric SAR speckle filtering and its implication for classification. *IEEE Transactions on Geoscience and Remote Sensing*, *37*(5), 2363–2373. https://doi.org/10.1109/36.789635

Lu, X., & Liu, F. (2012). Geostatistics and 3S Technology. *Remote Sensing, Environment and Transportation Engineering (RSETE), 2012 2nd International Conference*, 3–6. https://doi.org/10.1109/RSETE.2012.6260729

Marencic, H. (2009). The Wadden Sea - Introduction. Thematic Report No. 1. In H. Marencic & J. de Vlas (Eds.), *Quality Status Report 2009. Wadden Sea Ecosystem No. 25.* (p. 597). Wilhelmshaven, Germany. Retrieved from http://www.waddensea-secretariat.org/sites/default/files/downloads/qsr-2009.pdf

McNairn, H., & Shang, J. (2016). A Review of Multitemporal Synthetic Aperture Radar (SAR) for CropMonitoring. In Y. Ban (Ed.), *Multitemporal Remote Sensing* (1st ed., p. 445). Stockholm: Springer. https://doi.org/10.1007/978-3-319-47037-5

MDA. (2016). *RADARSAT-2 product description*. Richmond.

Melchionna, S., & Gade, M. (2014). SAR Observations for Oyster and Mussel Beds Detection in the German Wadden Sea. In *EuSAR* (pp. 705–707). Berlin, Germany.

Morris, E. P. (2005). *Quantifying primary production of microphytobenthos: Application of optical methods (PhD Thesis)*. University of Groningen.

Mumby, P. J., Green, E. P., Edwards, A. J., & Clark, C. D. (1997). Coral reef habitat mapping: how much detail can remote sensing provide? *Marine Biology*, 193–202. https://doi.org/https://doi.org/10.1007/s002270050238

Naimi, B., Skidmore, A. K., Groen, T. A., & Hamm, N. A. S. (2011). Spatial autocorrelation in predictors reduces the impact of positional uncertainty in occurrence data on species distribution modelling. *Journal of Biogeography*, *38*(8), 1497–1509. https://doi.org/10.1111/j.1365-2699.2011.02523.x

Nehls, G., & Büttger, H. (2007). *Spread of the Pacific Oyster Crassostrea gigas in the Wadden Sea: Causes and consequences of a successful invasion. The Common Wadden Sea Secretariat*. Wilhelmshaven, Germany.

Nehls, G., Diederich, S., Thieltges, D. W., & Strasser, M. (2006). Wadden Sea mussel beds invaded by oysters and slipper limpets: Competition or climate control? *Helgoland Marine Research*, *60*(2), 135–143. https://doi.org/10.1007/s10152-006-0032-9

Nehls, G., Hertzler, I., & Scheiffarth, G. (1997). Stable mussel Mytilus edulis beds in the Wadden Sea— They're just for the birds. *Helgoländer Meeresuntersuchungen*, *51*, 361–372. https://doi.org/10.1007/BF02908720

Nehls, G., & Thiel, M. (1993). Large-scale distribution patterns of the mussel (Mytilus edulis) in the Wadden Sea of Schleswig-Holstein: Do storms structure the ecosystem? *Netherlands Journal of Sea Research*, *31*(2), 181–187. https://doi.org/10.1016/0077-7579(93)90008-G

Nga, N. T. (2010). *Estimation and mapping of above ground biomass for the assessment and mapping of carbon stocks in tropical forest using SAR data:A case study in Afram headwaters forest, Ghana (MSc Thesis). University of Twente: Faculty of Geo-Information and Earth Observation (ITC)*. University of Twente. unpublished. Retrieved from https://www.itc.nl/library/papers_2010/msc/nrm/nga.pdf

Nieuwhof, S., Herman, P. M. J., Dankers, N., Troost, K., & Van Der Wal, D. (2015). Remote sensing of epibenthic shellfish using Synthetic Aperture Radar Satellite Imagery. *Remote Sensing*, *7*(4), 3710–3734. https://doi.org/10.3390/rs70403710

NIOZ. (2017). Netherlands Institute for Sea Research- NIOZ. Retrieved May 21, 2017, from https://www.nioz.nl/en/expertise/waddencentre

Poenaru, V., Badea, A., Cimpeanu, S. M., & Irimescu, A. (2015). Multi-temporal Multi-spectral and Radar Remote Sensing for Agricultural Monitoring in the Braila Plain. In *Agriculture and Agricultural Science Procedia* (Vol. 6, pp. 506–516). Bucharest, Romania: Elsevier Srl. https://doi.org/10.1016/j.aaspro.2015.08.134

Rijkswaterstaat. (n.d.). Home | Rijkswaterstaat. Retrieved February 19, 2018, from https://www.rijkswaterstaat.nl/

Roberts, C. M., Andelman, S., Branch, G., Bustamante, R. H., Castilla, J. C., Dugan, J., … Lafferty, K. D. (2003). Ecological Criteria for Evaluating Candidate Sites for Marine Reserves. *Ecological Applications*, *13*(1), 199–214. https://doi.org/10.1890/1051-0761(2003)013[0199:ECFECS]2.0.CO;2

Saleh, A. (1993). Soil Roughness Measurement - Chain Method. *Journal of Soil and Water Conservation*, *48*, 527–529.

Sundseth, K. (2014). The EU Birds and Habitats Directives. Luxembourg: EU. https://doi.org/10.2779/30198

Thorup, O., & Koffijberg, K. (2016). *Breeding success in the Wadden Sea 2009-2012 A review.* Wilhelmshaven, Germany. Retrieved from www.waddensea-secretariat.org

Tonye, E., Fotsing, J., Essimbi Zobo, B., Talla Tankam, N., Kanaa, T. F. N., & Rudant, J. P. (2011). Contribution of variogram and feature vector of texture for the classification of big size SAR images. In *Proceedings - 7th International Conference on Signal Image Technology and Internet-Based Systems, SITIS 2011* (pp. 382–389). Dijon: IEE. https://doi.org/10.1109/SITIS.2011.67

Troost, K. (2009). *University of Groningen Pacific oysters in Dutch estuaries (PhD Thesis).* University of Groningen.

van Den Ende, D., Brummelhuis, E., VanZweeden, C., Troost, K., & Van Asch, M. (2016). *Mosselbanken en oesterbanken op droogvallende platen in de Nederlandse kustwateren in 2016 : bestand en arealen.* Wageningen. Retrieved from http://edepot.wur.nl/369987

van der Wal, D., & Herman, P. M. J. (2007). Regression-based synergy of optical, shortwave infrared and microwave remote sensing for monitoring the grain-size of intertidal sediments. *Remote Sensing of Environment*, *111*(1), 89–106. https://doi.org/10.1016/j.rse.2007.03.019

van Roomen, M., Laursen, K., van Turnhout, C., van Winden, E., Blew, J., Eskildsen, K., … Ens, B. J. (2012). Signals from the Wadden sea: Population declines dominate among waterbirds depending on intertidal mudflats. *Ocean and Coastal Management*, *68*, 79–88. https://doi.org/10.1016/j.ocecoaman.2012.04.004

Veci, L. (2015). SENTINEL-1 Toolbox SAR Basics Tutorial. *Esa*. ESA. Retrieved from http://sentinel1.s3.amazonaws.com/docs/S1TBX SAR Basics Tutorial.pdf

Wang, W., Gade, M., & Yang, X. (2017). Detection of Bivalve Beds on Exposed Intertidal Flats Using Polarimetric SAR Indicators. *Remote Sensing*, *9*(10). https://doi.org/10.3390/rs9101047

White, L., Brisco, B., Dabboor, M., Schmitt, A., & Pratt, A. (2015). *A collection of SAR methodologies for monitoring wetlands. Remote Sensing* (Vol. 7). MDPI. https://doi.org/10.3390/rs70607615

Wolff, W. J., Bakker, J. P., Laursen, K., & Reise, K. (2010). *The Wadden Sea Quality Status Report - Synthesis Report 2010.* Wilhelmshaven, Germany.

World Numismatic News. (2017). 2016 Commemorative Silver and Gold from Netherlands. Retrieved August 21, 2017, from http://worldnumismaticnews.com/2016/05/18/2016-commemorative-silver-and-gold-from-netherlands/

Wu, S., Xu, B., & Wang, L. (2006). Urban Land-use Classification Using Variogram-based Analysis with an Aerial Photograph. *Photogrammetric Engineering & Remote Sensing*, *72*(7), 813–822. https://doi.org/10.14358/PERS.72.7.813

APPENDICES

Appendix 1:Field Instruments and Images

Field Materials	Purpose	Source
Steel chain 10m and 1m	Surface roughness Measurement	ITC
Measuring Tape	30m	
Garmin GPS	Navigation and geolocation	
IPAQ Pocket PC: error of 2m	Location of sample points	
Compass	Aligning to North pole	
Aerial Photographs(2014, 2015,2016,2017)	Visual interpretation of shellfish bed cover estimation	ArcGIS Online (Luchfoto)
Multiple SAR Images (2016,2017)	Shellfish differentiation and density distribution	Technical University of Delft
1. Radarsat-2 scenes 2. Sentinel 1 scenes	Shellfish differentiation and density distribution	Technical University of Delft
3. Wadden Sea (vector) contour maps (2016)	Mussel beds and Oyster reefs distribution	Wageningen University; IMARES
Fieldwork data sheet	Field data recorded	Constructed
Low tide scenes	Field data collection time	Rijkswaterstaat

Appendix 2: Softwares

Software	Purpose
Arc GIS	Map construction Arc GIS ONLINE (Aerial Photos retrieval and interpretation)
Erdas IMAGINE	Time series Analysis
SNAP Toolbox	Image processing (Radiometric, co-registration and speckle filtering) cluster analysis
	Statistical Analysis of Data
R programming language Microsoft office Excel	
Microsoft office Word	
	Research Writing

Appendix 3: Data Collection Sheet Wadden Sea

| Stratum		Date:	GPS	X						
Sample Site :		Time:	RD	Y						
Patch Pattern		Homogenous			Mosaic					
Sample Plot size:										
Chain Measurement		Overall ruggedness								
		10M : NS :		10M: WE :						
		1M : NS :		1M: WE :						
Shellfish Height measurement from the sediment (m)										
Sediments		Sand		Clay			Silt			
Cover		Percentage								
Shellfish Beds	Crassostrea gigas									
	Blue M. edulis									
Mixed shellfish Beds										
Dead shells										
Sea weed , sea grass										
Water										
Photograph										
Comments /Observations										

Appendix 4: Descriptive statistics of shellfish species and density with different polarisations of two types of satellites

ID	Mussel	Oyster	total shellfish	class	JULY_VV	MAY_VV	Sentinel_HH	Sentinel_HV
A1	20	65	85	oyster	-6.87682	-7.14563	-4.79641	-14.8581
A2	0	30	30	oyster	-10.2439	-7.74091	-6.85317	-19.0681
A3	1	3	4	scattered shellfish	-17.5122	-13.1027	-13.6515	-20.7523
A4	80	0	80	mussel	-3.69899	-11.0655	-10.1279	-18.8334
A5	0	10	10	oyster	-9.69487	-11.9224	-10.2668	-18.7424
B1	15	35	50	oyster	-6.06809	-6.48571	-6.79942	-12.982
B10	3	7	11	scattered shellfish	-10.9369	-11.6927	-8.32483	-19.931
B2	15	20	35	mixed shellfish	-7.97645	-7.4395	-6.2894	-14.5668
B3	5	15	20	oyster	-12.2852	-10.9859	-14.2767	-20.6421
B4	0	80	80	oyster	-8.20365	-5.89105	-5.9189	-14.3301
B6	0	1	1	sediment	-13.9278	-16.5999	-16.8195	-21.5742
B7	0	5	5	scattered shellfish	-15.8213	-12.0335	-16.6275	-21.1412
B8	0	0	0	sediment	-17.835	-17.6606	-14.2482	-21.0709
B9	10	20	50	mixed shellfish	-8.3161	-9.24524	-3.99352	-18.6396
H1	10	0	20	mussel	-12.0367	-10.8714	-12.3177	-19.2503
H2	20	1	26	mussel	-10.5393	-4.09397	-8.59463	-16.7896
H3	19	1	20	mussel	-5.57977	-8.71684	-6.60778	-17.3596
H4	0	0	0	sediment	-20.5414	-18.9396	-18.7746	-20.5313
H5	10	1	16	mussel	-9.14373	-6.00232	-9.32659	-19.2015
H6	0	0	0	sediment	-17.1557	-13.0456	-13.7322	-19.8179
H7	15	0	16	mussel	-8.2108	-9.50882	-9.18779	-17.5498
H8	10	0	20	mussel	-11.8834	-9.47603	-12.5158	-19.4852
M1	25	0	25	mussel	-10.2536	-9.7468	-7.44076	-16.9369
M2	80	1	81	mussel	-6.19764	-10.5126	-8.40222	-16.4123
M3	20	0	20	mussel	-9.12509	-11.5297	-9.82986	-19.159
M4	2	0	2	scattered shellfish	-11.2851	-14.3924	-9.53996	-19.5289
M5	0	0	0	sediment	-19.7516	-15.8184	-13.2991	-20.6719
P1	1	85	86	oyster	-5.33172	-5.89963	-7.88542	-18.2911
p2	1	9	10	oyster	-18.5456	-12.1579	-13.1556	-21.4142
P3	0	70	70	oyster	-4.2276	-5.27279	-6.39881	-15.0497
P4	0	0	0	sediment	-14.9146	-19.1911	-12.9635	-20.889
p5	0	3	3	scattered shellfish	-17.5166	-16.3909	-14.2622	-20.6669
P6	0	0	0	sediment	-18.2478	-18.105	-16.2216	-20.9642
P7	0	0	0	sediment	-14.6078	-17.9171	-16.0321	-21.3453
P8	5	5	10	mixed shellfish	-5.70337	-8.40954	-7.51225	-14.7642
P9	10	5	15	mussel	-8.77927	-9.56121	-9.39456	-16.4236
R1	0	15	15	oyster	-6.48893	-10.2039	-7.12885	-13.8486
R2	40	0	50	mussel	-12.8003	-15.2255	-6.85797	-15.1209
R3	0	0	0	sediment	-5.53424	-10.4815	-13.8967	-19.9324
R4	55	0	65	mussel	-6.73753	-5.85218	-5.49377	-16.5803

Appendix 4: Shellfish species and density with different polarisations of two types of satellites

ID	Mussel	Oyster	total shellfish(%)	class	_JULY_VV	MAY_VV	Sentinel_HH	Sentinel_HV
R5	20	0	20	mussel	-8.75272	-9.91408	-8.48602	-19.2273
R6	0	0	0	sediment	-20.4881	-15.7603	-15.4758	-20.7588
T1	16	25	41	mixed shellfish	-4.26202	-7.63304	-5.50617	-17.8704
T2	40	50	90	mixed shellfish	-4.68028	-9.08067	-5.35088	-11.6174
T3	5	25	35	oyster	-5.3618	-7.68604	-5.48613	-16.3947
T4	0	0	0	sediment	-16.2945	-17.7914	-17.7263	-20.9563
T5	0	0	0	sediment	-17.5582	-19.0431	-17.7301	-21.3839
T6	0	0	0	sediment	-20.1921	-15.1429	-13.8329	-20.9916
T7	0	0	0	sediment	-14.3554	-13.698	-17.9097	-21.2082
T8	0	0	0	sediment	-14.1862	-14.7272	-13.8029	-20.2242

Appendix 5: Estimated sediment types with their dB values along the tidal flats in RSC VV
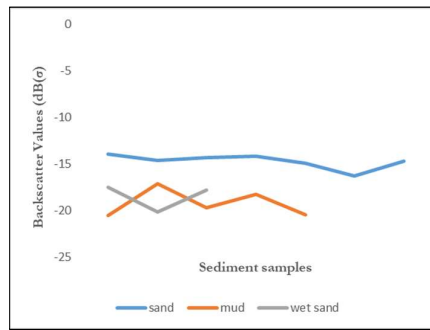
Appendix 6 : Scatterplot showing the relation between RS2 images of July VV polarized data and May VV polarized data.
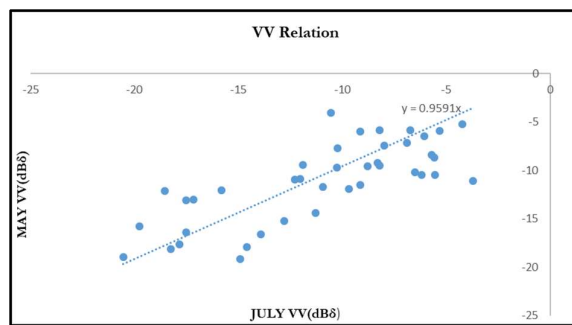
Appendix 7: Relationship between shellfish density and Mean VV backscatter values
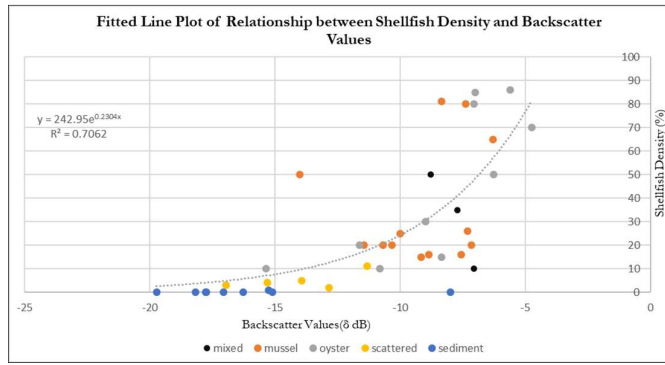
Fitted Line Plot of Relationship between Shellfish Density and Backscatter Values

$y = 242.95e^{0.2304x}$
$R^2 = 0.7062$

● mixed ● mussel ● oyster ● scattered ● sediment

Backscatter Values(δ dB)

Shellfish Density (%)

Appendix 8: Spherical model fit in semi-variance analysis with 50 sample plots field parameters

SITE	X	Y	range	Sill	Shellfish (%)	class	Rugosity	Height(m)	RMSE
A1	178294	605627	6.458	0.0066	85	oyster	0.075	8.16	0.072
A2	178106	605667	10.979	0.0008	30	oyster	0.047	7.16	0.01
A3	178054	605759	7.763	0.0124	7	scattered shellfish	0.0075	6.5	0.001
A4	178051	606069	10.792	0.0288	80	mussel	0.005	2	0.069
A5	178027	605855	8.0226	0.0011	10	oyster	0	0	0.018
B1	148657	597503	9.1545	0.0036	50	oyster	0.042	6.55	0.030
B10	151507	599330	220.43	0.0031	11	scattered shellfish	0	0	0.015
B2	148802	597472	9.1576	0.0142	35	mixed shellfish	0.0575	7.5	0.054
B3	148852	597537	9.9056	0.0010	20	oyster	0	0	0.014
B4	151564	598566	13.418	0.0082	80	oyster	0.078	12.4	0.045
B6	149545	597729	9.7499	0.0005	1	sediment	0	0	0.011
B7	151556	598682	12.289	0.0001	5	scattered shellfish	0	0	0.004
B8	151528	598875	152.867	0.0234	0	sediment	0	0	0.023
B9	151696	599184	7.119	0.0029	50	mixed shellfish	0	0	0.034
H1	192381	601624	6.357	8.37E-05	20	mussel	0.016	1.6	0.006
H2	192375	601777	7.449	0.0035	26	mussel	0.02	2.8	0.04
H3	192669	601815	7.449	0.0035	20	mussel	0.008	1.9	0.04
H4	192870	601470	8.525	1.21E-05	0	sediment	0	0	0.002
H5	192370	601701	6.685	0.00042	16	mussel	0	0	0.012
H6	192368	601724	5.154	0.000381	0	sediment	0	0	0.016
H7	192369	601743	8.145	0.0004	16	mussel	0	0	0.011
H8	192721	601730	7.477	0.0044	20	mussel	0	0	0.034
M1	199918	602910	9.620	0.0007	45	mussel	0.007	2	0.01
M2	199876	603272	10.19	0.0309	81	mussel	0.011	3.5	0.075
M3	200036	603258	8.265	0.0022	20	mussel	0.007	2	0.018
M4	200028	603307	7.038	0.0003	2	scattered shellfish	0.002	4	0.01
M5	200004	602978	14.01	7.60E-06	0	sediment	0	0	0.002434
P1	145705	597537	168.31	0.127529	86	oyster	0.0985	8.833333	0.073233
P2	145875	597519	7.8561	1.85E-05	10	oyster	0.0145	5.4	0.003331
P3	145306	597432	83.816	0.01547	70	oyster	0.5325	12.75	0.068662
P4	145681	597774	11.051	0.005	0	sediment	0	0	0.021854
P5	145818	597464	6.226	7.58E-06	3	scattered shellfish	0	0	0.001961
P6	145837	597740	353.52	0.005	0	sediment	0	0	0.005097
P7	145629	597741	7.92	0.003	0	sediment	0	0	0.033435
P8	144326	597548	8.30	0.010	70	mixed shellfish	0	0	0.040673
P9	144217	597515	78.69	0.003	70	mussel	0	0	0.032361
R1	215220	602284.6	12.6	0.04	15	oyster	0	0	0.098384
R2	215560.2	603135.5	10.69	0.008	50	mussel	0.006	0	0.049045
R3	215408.2	602664.8	6.052	0.0001	0	sediment	0.003	0	0.007858
R4	193950.9	601866.6	7.763	0.012	65	mussel	0.0085	0	0.071176

Appendix 8: Spherical model fit in semi-variance analysis with 50 sample plots field parameters									
R5	200395.3	603107.2	8.389	0.0008	20	mussel	0.0055	0	0.012234
R6	200414.7	602886.7	421.39	0.0006	0	sediment	0.00275	0	0.00229
T1	147338	597599	6.464	0.134	41	mixed shellfish	0.0245	8.6	0.251967
T2	147261	597626	30.635	0.0808	90	mixed shellfish	0.043	10.2	0.091703
T3	147121	597538	19.02	0.0088	35	oyster	0.027	10.75	0.046405
T4	147435	598080	351	0.0014	0	sediment	0	0	0.004795
T5	147407	597946	8.53	0.0001	0	sediment	0	0	0.005921
T6	147191	597791	9.77	2.20E-05	0	sediment	0	0	0.003369
T7	147295	598009	5.27	0.0002	0	sediment	0	0	0.011645
T8	147392	598257	10.8	0.0003	0	sediment	0	0	0.008001

Appendix 9: Exponential model fit in semi-variance analysis with 50 sample plots field parameters

SITE	X	Y	range	psill	nugget	shellfish(%)	Height(cm)	class
A1	178294	605627	10	0	0.004	85	8.16	oyster
A2	178106	605667	10	0	0.004	30	7.16	oyster
A3	178054	605759	10	0	0.004	7	6.5	scattered
A4	178051	606069	9.15	0.042	0.004	80	2	mussel
A5	178027	605855	10	0	0.004	10	0	oyster
B1	148657	597503	10	0	0.00004	50	6.55	oyster
B10	151507	599330	1146.9	2.81E-02	0.00004	11	0	scattered
B2	148802	597472	6.09	0.018	0.00004	35	7.5	Mixed shellfish
B3	148852	597537	10	0	0.00004	20	0	oyster
B4	151564	598566	14.71	0.015	0.00004	80	12.4	oyster
B6	149545	597729	6.700	0.0006	0.00004	1	0	Sediment shellfish
B7	151556	598682	12.72	0.000	0.00004	5	0	scattered shellfish
B8	151528	598875	654.8	0.208	0.00021	0	0	sediment
B9	151696	599184	10	0	0.00004	50	0	mixed
H1	192381	601624	10	0	2.13E-06	20	1.6	mussel
H2	192375	601777	10	0	0.00004	26	2.8	mussel
H3	192669	601815	10	0	0.00004	20	1.9	mussel
H4	192870	601470	10	0	0.00004	0	0	sediment
H5	192370	601701	10	0	0.00001	16	0	mussel
H6	192368	601724	10	0	4.01E-05	0	0	sediment
H7	192369	601743	10	0	0.00001	16	0	mussel
H8	192721	601730	10	0	0.00004	20	0	mussel
M1	199918	602910	10	0	0.00004	45	2	mussel
M2	199876	603272	6.80159	0.03	0.00004	81	3.5	mussel
M3	200036	603258	10	0	0.00004	20	2	mussel
M4	200028	603307	10	0	0.00004	2	4	scattered
M5	200004	602978	6.603244	1.02	2.46138E-06	0	0	sediment
P1	145705	597537	497.4989	0.656	0.00004	86	8.8	oyster
P2	145875	597519	10	0	0.00004	10	5.4	oyster
P3	145306	597432	5.352536	0.016	0.00004	70	12.75	oyster
P4	145681	597774	10.85485	0.009	0.00004	0	0	sediment
P5	145818	597464	10	0	0.00004	3	0	scattered
P6	145837	597740	1436.718	0.039	0.00004	0	0	sediment
P7	145629	597741	0.00341507	0.003	0.00004	0	0	sediment
P8	144326	597548	4.280679	0.012	0.00004	70	0	mixed
P9	144217	597515	12.16722	0.006	0.00004	70	0	mussel

R1	215220	602285	14.439	0.086	0.00004	15	0	oyster
R2	215560	603135	8.543	0.012	0.00004	50	0	mussel
R3	215408	602665	10	0	0.00004	0	0	sediment
R4	193951	601867	10	0	0.00004	65	0	mussel
R5	200395	603107	10	0	0.00004	20	0	mussel
R6	200415	602887	2444.98	0.005	0.00004	0	0	sediment
T1	147338	597599	23.53887	0.131	0.00316	41	8.6	mixed
T2	147261	597626	151.4137	0.598	0.00004	90	10.2	mixed
T3	147121	597538	34.41697	0.025	0.00004	35	10.75	oyster
T4	147435	598080	1.77E+03	1.25E-02	8.06472E-06	0	0	sediment
T5	147407	597946	10	0	0.00004	0	0	sediment
T6	147191	597791	6.180651	2.89E-05	6.84724E-07	0	0	sediment
T7	147295	598009	10	0	0.00004	0	0	sediment
T8	147392	598257	10	0.00E+00	0.00004	0	0	sediment

Appendix 10:Stepwise (backward) regression results

Field Parameters	Stepwise Regression Results

Rugosity	Start: AIC=-252.73
	d$Rugosity ~ d$range + d$psill
	
	           Df Sum of Sq RSS AIC
	- d$range 1 0.0004114 0.28335 -254.66
	- d$psill 1 0.0067781 0.28971 -253.54
	<none> 0.28294 -252.73
	
	Step: AIC=-254.66
	d$Rugosity ~ d$psill
	
	           Df Sum of Sq RSS AIC
	- d$psill 1 0.0070144 0.29036 -255.43
	<none> 0.28335 -254.66
	
	Step: AIC=-255.43
	d$Rugosity ~ 1

Shellfish Height	Start: AIC=330.38
	d$shellfish... ~ d$range + d$psill
	
	          Df Sum of Sq RSS AIC
	- d$range 1 1261.4 34111 330.27
	<none> 32850 330.38
	- d$psill 1 9340.4 42190 340.90
	
	Step: AIC=330.27
	d$shellfish... ~ d$psill
	
	          Df Sum of Sq RSS AIC
	<none> 34111 330.27
	- d$psill 1 8953.1 43064 339.92

Shellfish Density	Start: AIC=126.7
	d$Height.m. ~ d$range + d$psill
	
	          Df Sum of Sq RSS AIC
	- d$range 1 11.416 570.39 125.72
	<none> 558.97 126.70
	- d$psill 1 154.411 713.39 136.90
	
	Step: AIC=125.71
	d$Height.m. ~ d$psill
	
	          Df Sum of Sq RSS AIC
	<none> 570.39 125.72
	- d$psill 1 149.81 720.20 135.38

Appendix 11 : Multiple Regression of Rugosity with Range and sill

SUMMARY OUTPUT								
Regression Statistics								
Multiple R	0.578511							
R Square	0.334675							
Adjusted R Square	0.268143							
Standard Error	0.092956							
Observations	23							
ANOVA								
	df	*SS*	*MS*	*F*	*Significance F*			
Regression	2	0.086931	0.043466	5.030254	0.016995607			
Residual	20	0.172817	0.008641					
Total	22	0.259749						
	Coefficients	*Standard Error*	*t Stat*	*P-value*	*Lower 95%*	*Upper 95%*	*Lower 95.0%*	*Upper 95.0%*
Intercept	0.02797	0.023169	1.207197	0.24144	-0.020360483	0.076301	-0.02036	0.076301
range	0.002103	0.000667	3.153978	0.004993	0.000712276	0.003495	0.000712	0.003495
sill	-0.94807	0.626113	-1.51422	0.145615	-2.254120862	0.357978	-2.25412	0.357978

Appendix 12: Multiple regression between Shellfish Density with Range and Sill

SUMMARY OUTPUT								
Regression Statistics								
Multiple R	0.483294							
R Square	0.233573							
Adjusted R Square	0.156931							
Standard Error	26.21968							
Observations	23							
ANOVA								
	df	*SS*	*MS*	*F*	*Significance F*			
Regression	2	4190.222	2095.111	3.047561	0.069937			
Residual	20	13749.43	687.4715					
Total	22	17939.65						
	Coefficients	*Standard Error*	*t Stat*	*P-value*	*Lower 95%*	*Upper 95%*	*Lower 95.0%*	*Upper 95.0%*
Intercept	36.72587	6.535272	5.619639	1.68E-05	23.09353	50.35821	23.09353	50.35821
range	0.206793	0.188113	1.099301	0.284694	-0.1856	0.599191	-0.1856	0.599191
sill	211.1274	176.6045	1.195481	0.245882	-157.263	579.5179	-157.263	579.5179

Appendix 13 : Multiple Regression of Shellfish Height with range and sill

SUMMARY OUTPUT								
Regression Statistics								
Multiple R	0.432418							
R Square	0.186985							
Adjusted R Square	0.105684							
Standard Error	3.802044							
Observations	23							
ANOVA								
	df	*SS*	*MS*	*F*	*Significance F*			
Regression	2	66.49253	33.24626	2.299898	0.126178			
Residual	20	289.1108	14.45554					
Total	22	355.6033						
	Coefficients	*Standard Error*	*t Stat*	*P-value*	*Lower 95%*	*Upper 95%*	*Lower 95.0%*	*Upper 95.0%*
Intercept	4.312654	0.947662	4.550837	0.000194	2.335866	6.289443	2.335866	6.289443
range	0.032485	0.027278	1.190906	0.247633	-0.02442	0.089386	-0.02442	0.089386
sill	20.28396	25.60893	0.792066	0.437617	-33.1353	73.70326	-33.1353	73.70326

Appendix 14 : HV image obtained from merging HH (SC1) and VV(RSC2) polarized data
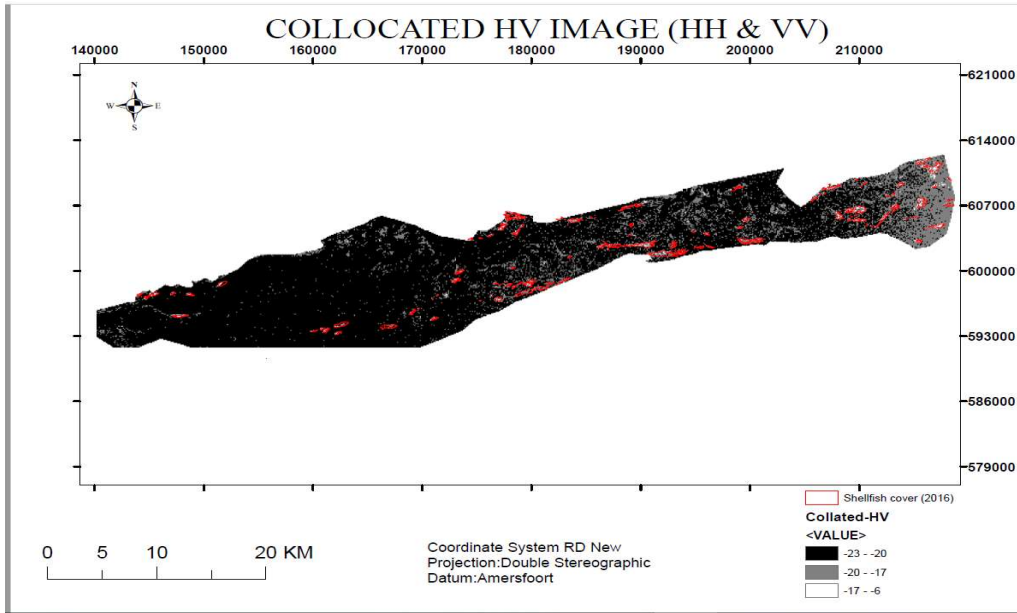
Appendix 15: Results of Variogram Analysis of a 2km by 2km subset

np	dist		semi-variance ((γ)
1	13057864	33.50	0.3332351
2	38355898	77.90	0.7407981
3	60930278	126.57	0.9715225
4	83813914	175.97	1.1081957
5	103980791	225.81	1.1867564
6	123977097	275.84	1.2314211
7	139961966	325.80	1.2634461
8	154958886	375.35	1.3069845
9	171966042	425.16	1.3501670
10	185542782	475.34	1.3818111
11	196159674	525.35	1.3976204
12	208628498	575.42	1.3995655
13	214405236	625.27	1.4164597
14	224389832	674.94	1.4464855
15	233226985	725.03	1.4785234
16	237004476	775.11	1.5099913
17	242506241	825.09	1.5544855
18	244267768	875.01	1.6054863
19	247275590	924.84	1.6599675
20	250973230	975.004	1.7169549

Appendix 16: Summary of Linear regression statistics between backscatter values and Shellfish Density

Radar Image	R²	P-Value	Standard Error(db)
14th May 2017 RSC-VV 18: 21	0.47	3.93E-08	3.10
25th July 2017 RSC-VV 18:20	0.53	1.43E-09	3.6
9th June 2016 Sentinel HH 18:20	0.57	1.97E-10	2.8
9th June 2016 Sentinel HV 18: 20	0.61	1.91E-11	1.6